A&A 453, 261–278 (2006)
DOI: 10.1051/0004-6361:20053065

Astronomy & Astrophysics

Rotational mixing in low-mass stars

II. Self-consistent models of Pop II RGB stars

A. Palacios[1], C. Charbonnel[2,3], S. Talon[4], and L. Siess[1]

[1] Institut d'Astronomie et d'Astrophysique, Université Libre de Bruxelles Campus de la Plaine, Boulevard du Triomphe, CP 226, 1050 Bruxelles, Belgium
e-mail: apalacio@ulb.ac.be; ana.palacios@cea.fr
[2] Observatoire de Genève, 51 chemin des Maillettes, 1290 Sauverny, Switzerland
[3] Laboratoire d'Astrophysique de Toulouse-Tarbes, Observatoire Midi-Pyrénées, 14 Av. E. Belin, 31400 Toulouse, France
[4] Département de Physique, Université de Montréal, Montréal PQ H3C 3J7, Canada

Received 15 March 2005 / Accepted 21 February 2006

ABSTRACT

Aims. In this paper we study the effects of rotation in low-mass, low-metallicity RGB stars.
Methods. We present the first evolutionary models taking into account self-consistently the latest prescriptions for the transport of angular momentum by meridional circulation and shear turbulence in stellar interiors as well as the associated mixing processes for chemicals computed from the ZAMS to the upper RGB. We discuss the uncertainties associated with the physical description of the rotational mixing in detail and carefully study their effects on the rotation profile, diffusion coefficients, structural evolution, lifetimes, and chemical signatures at the stellar surface. We focus in particular on the various assumptions concerning the rotation law in the convective envelope, the initial rotation velocity distribution, the presence of μ-gradients, and the treatment of the horizontal and vertical turbulence.
Results. This exploration leads to two main conclusions. (1) After completion of the first dredge-up, the degree of differential rotation (and hence mixing) is maximised in the case of a differentially rotating convective envelope (i.e., $j_{\rm CE}(r)$ = const.), as anticipated in previous studies. (2) Even with this assumption, and contrary to some previous claims, the present treatment for the evolution of the rotation profile and associated meridional circulation and shear turbulence does not lead to enough mixing of chemicals to explain the abundance anomalies in low-metallicity field and globular cluster RGB stars observed around the *bump* luminosity.
Conclusions. This study raises questions that need to be addressed in the near future. These include, for example, the interaction between rotation and convection and the trigger of additional hydrodynamical instabilities.

Key words. stars: evolution – stars: interiors – stars: rotation – stars: abundances – hydrodynamics – turbulence

1. Abundance anomalies in RGB stars

The standard theory of stellar evolution[1] predicts that the chemical composition on the surface of low-mass stars is modified on the way to the red giant branch (RGB) during the so-called first dredge-up (hereafter 1st DUP; Iben 1965). There, the expanding stellar convective envelope (hereafter CE) deepens in mass, leading to dilution of the surface material within regions that have undergone partial hydrogen burning in the earlier main sequence. Qualitatively, this leads to a decrease in the surface abundances of the fragile LiBeB elements and of ^{12}C, while those of ^{3}He, ^{13}C, and ^{14}N increase. Abundances of O and heavier elements essentially remain unchanged. Quantitatively, these abundance variations depend on the stellar mass and metallicity (e.g., Sweigart et al. 1989; Charbonnel 1994; Boothroyd & Sackmann 1999). After the 1st DUP, the CE withdraws, while the hydrogen burning shell (hereafter HBS) moves outward in mass. Within the standard framework no more variations of the surface abundance pattern are expected until the star reaches the asymptotic giant branch (hereafter AGB).

Observations sampling the evolution from the turn-off to the base of the RGB in open clusters and in the galactic field stars have validated these predicted surface abundance variations up to the completion of the 1st DUP[2] (e.g. Gratton et al. 2000). However, observational evidence has accumulated of a second and distinct mixing episode that is not predicted by standard models and that occurs in low-mass stars after the end of the 1st DUP and, more precisely, at the RGB *bump*.

The determination of the carbon isotopic ratio ^{12}C/^{13}C (hereafter *CIR*) for RGB stars in open clusters with various turn-off masses (Gilroy 1989) has provided the first pertinent clue to this process. It was indeed shown that bright RGB stars with initial masses lower than ∼2−2.5 $M_{\odot}$ exhibit considerably lower *CIR* than predicted by standard models after the 1st DUP. Thanks to data collected in stars sampling the RGB of M 67 (Gilroy & Brown 1991), it clearly appeared that observations deviate from standard predictions just at the so-called RGB *bump* (Charbonnel 1994). The Hipparcos parallaxes allowed the evolutionary phase of large samples of field stars with known *CIR* to

[1] By this we refer to the modelling of non-rotating, non-magnetic stars, in which convection and atomic diffusion are the only transport processes considered.

[2] One has, of course, to consider possible variations in the surface abundance of lithium occurring in some cases already on the main sequence (hereafter MS). This discussion is, however, beyond the scope of this paper (see e.g. Charbonnel et al. 2000; and Palacios et al. 2003, Paper I).

be precisely determined. These stars were found to behave similarly to those in M 67; e.g. they presented unpredictedly low *CIR* appearing at the RGB *bump* luminosity (Charbonnel et al. 1998; Gratton et al. 2000).

On the other hand, the region around the *bump* has also been probed for two globular clusters (GCs). In NGC 6528 and M4 again, the *CIR* drops below the 1st DUP standard predictions just at the RGB *bump* (Shetrone 2003a,b). Moreover, all the brightest RGB stars observed so far in globular clusters exhibit *CIR* close to the equilibrium value of the CN cycle.

During this second mixing episode, surface abundances of other chemical elements are also affected both in field and GCs giants: Li decreases at the RGB *bump* (Pilachowski et al. 1993; Grundahl et al. 2002). C decreases, while N increases for RGB stars brighter than the *bump* (Gratton et al. 2000; Bellman et al. 2001, and references therein), confirming the envelope pollution by CN processing. In the case of GCs, this picture is, however, blurred by the probable non-negligible dispersion of the initial [C/Fe]. As far as lithium, carbon isotopes, and nitrogen are concerned, the abundance variations on the upper RGB have similar amplitudes in field and globular cluster giants (Smith & Martell 2003). The finding that the so-called super Li-rich giants (Wallerstein & Sneden 1982) all lie either at the RGB *bump* or on the early-AGB (Charbonnel & Balachandran 2000), certainly indicates the occurrence of an extra-mixing episode at these evolutionary points. The triggering of this mixing episode has been suggested as having an external nature external nature (Denissenkov & Herwig 2004), but it is more likely related to the aforementioned second mixing episode, which would start with a Li-rich phase as proposed by Palacios et al. (2001).

For more than a decade it has been known that, in addition to the elements discussed previously, O, Na, Mg, and Al also show variations in GC red giants (Kraft et al. 1993; Ivans et al. 1999; Ramirez & Cohen 2002). As in the case of lighter nuclei, an in situ mixing mechanism was frequently invoked to explain these abundance anomalies and, in particular, the O-Na anti-correlation. For a long time this specific pattern could only be observed in the brightest GC RGB stars. However, O and Na abundances have recently been determined with 8–10 m class telescopes in lower RGB and in turn-off stars for a couple of GCs (for recent reviews, see Sneden 2005; and Charbonnel 2005, and references therein), revealing exactly the same O-Na anti-correlation as in bright giants.

This result is crucial. Indeed, the NeNa-cycle does not operate in MS low-mass stars, as the involved reactions require high temperatures that can only be reached on the RGB. The existence of the same O-Na anti-correlation on the MS and on the RGB in these clusters thus proves that this pattern does not result from self-enrichment. Recent determination of oxygen isotopic ratios in a few RGB stars with low *CIR* (Balachandran & Carr 2003) reinforces this result. These objects indeed present high $^{16}O/^{17}O$ and $^{16}O/^{18}O$ ratios, in agreement with extensive CN-processing but no dredge-up of ON-cycle material. The O-Na anti-correlation is generally assumed to have a primordial origin, even though it has proved difficult to find stellar candidates able to produce it (Decressin & Charbonnel 2005; Denissenkov & Herwig 2003). Let us finally mention the peculiar case of the M13 bright giants, where O, Na, Mg, and Al abundances appear to vary with luminosity. In this cluster the observed O-Na anti-correlation could thus be the result of a superimposition of self-enrichment with a primordial pattern (Johnson et al. 2005).

In short, observations provide definitive clues to an additional mixing episode occurring in low-mass stars after the end of the 1st DUP. This process appears to be universal and independent of the stellar environment, as it affects more than 95% of the low-mass stars (Charbonnel & do Nascimento 1998), whether they belong to the field, to open, or globular clusters. Some indications of such a process have also been detected in the brightest RGB stars of external galaxies like the LMC (Smith et al. 2002) and Sculptor (Geisler et al. 2005). Its chemical signatures are clear: the Li and ^{12}C abundances, as well as the $^{12}C/^{13}C$ ratio, drop while the ^{14}N and the $^{16}O/^{18}O$ ratio increase. These data attest to the presence of a non-standard mixing process connecting the stellar convective envelope with the external layers of the HBS where CN-burning occurs. Last but not least, they indicate that the effects of this process on surface abundances appear when the star reaches the RGB *bump*.

Why should the RGB *bump* be such a special evolutionary point in the present context? After the completion of the 1st DUP, the CE retreats to leave a discontinuity of mean molecular weight (or μ-barrier) at the mass coordinate of its maximum penetration. Subsequently, when the HBS eventually crosses this discontinuity, the star suffers a structural re-adjustment due to the composition changes (more H is made available in the burning shell). The resulting alteration of the energetics causes a momentary decrease in the stellar luminosity. This results in a higher probability of finding a star in this brightness bin, and translates into a *bump* in the luminosity functions of globular clusters. Standard theory and observations nicely agree on the size and the location of the *bump* in the HRD (e.g., Zoccali et al. 1999).

As for mixing in radiative stellar interiors, it was suggested that the discontinuity of molecular weight left by the 1st DUP could inhibit any extra-mixing between the base of the convective envelope and the HBS. After the *bump*, the μ-gradients are much smoother in this region, permitting some extra-mixing to occur (Sweigart & Mengel 1979; Charbonnel 1995; Charbonnel et al. 1998).

2. From the pioneering work on stellar rotation to the present treatment of the transport of angular momentum and chemicals

Sweigart & Mengel (1979, hereafter SM79) investigated the possibility that meridional circulation might lead to the mixing of CNO-processed material in RGB stars. Though the physics of rotation-induced mixing invoked at that time was very crude, this pioneering work has settled the cause of a complex problem magnificently. SM79 discussed the problem of μ-gradients in great detail, which were known to inhibit meridional circulation (Mestel 1953, 1957). They underline the necessity for the radiative zone separating the CE from the HBS not to present significant molecular weight gradients, so that the mixing will be efficient. The other crucial point made by SM79 concerns the importance of the angular momentum (hereafter AM) distribution within the deep CE of RGB stars on the resulting mixing of CNO-processed material. Indeed, beyond the 1st DUP, the angular velocity of a radiative layer near the HBS is sensitive to how much AM has been deposited by the retreating CE. SM79 investigated two extreme cases, namely (a) constant specific angular momentum and (b) uniform angular velocity within the CE. Substantial CNO processing of the envelope could be obtained with plausible MS angular velocity only when the inner part of the convection envelope was allowed to depart from solid body rotation. As we shall see in this paper, our lack of knowledge of the distribution of angular momentum within the CE of giant

stars remains one of the weakest points of our global understanding of rotation-induced mixing at this phase.

Rotational transport processes cannot be simply reduced to meridional circulation. Once established, this large-scale circulation generates advection of AM, and thus favours the development of various hydrodynamical instabilities. Zahn (1992) proposed a description of the interaction between meridional circulation and shear turbulence, pushing forward the idea of chocking the meridional circulation by μ-gradients. Following these developments but using a simplified version of Zahn's description, Charbonnel (1995) re-investigated the influence of such a process on RGB stars. She conjectured that the combination of the disappearance of the mean molecular weight gradient barrier after the *bump* and the increase of mixing in the HBS has the proper time dependence to account for the observed behaviour of carbon isotopic ratios and for the Li abundances in Population II low-mass giants.

In these exploratory computations, however, the diffusion coefficient for chemicals was derived from an assumed constant rotation velocity (in the radiative zone) on the RGB, and the transport of AM by hydrodynamical processes was not considered. This is, however, of utmost importance for understanding the rotation-induced mixing (see the review by Maeder & Meynet 2000).

Then, Denissenkov & Tout (2000) applied the formalism of Maeder & Zahn (1998) to a typical globular cluster RGB star. However, this was done in a post-processing approach and thus, did not take the feedback of mixing on the stellar structure into account. Considering the angular velocity at the base of the CE as a free adjustable parameter and treating the transport of chemicals only beyond the *bump* as in the aforementioned works, they obtained large diffusion coefficients able to reproduce not only the Li, C, and N abundance anomalies at the *bump*, but also the O-Na and Mg-Al anti-correlations. As these two features clearly have a primordial origin, Denissenkov & VandenBerg (2003) revised these results. They simplified their previous approach, letting AM evolve only with structural readjustments (no rotational transport), and derived a diffusion coefficient to be applied to the chemicals beyond the *bump*. They considered the resulting mixing rate to have "*the correct order of magnitude*", even though it is too low by a factor of 7 to reproduce the observational data for Pop I stars.

In the present paper we propose a self-consistent approach of rotational-mixing in low-mass RGB stars. We define here as self-consistent a model in which the transport of angular momentum and of chemicals is coupled to the evolution of the star from the zero-age main sequence on. If meridional circulation and shear-induced turbulence are the only transport processes of AM being considered, the assumptions made on the rotation profile solely concern the initial condition, i.e. the rotation profile at the ZAMS (assumed to be uniform) and the rotation regime in the convective envelope. At each evolutionary step, we thus compute the new rotation profile together with the associated transport coefficients resulting from structural readjustments and transport processes associated with rotation. The abundance profile of each chemical is then modified under the effect of both mixing and nuclear reactions. In such a procedure, the stellar structure "reacts" to rotational-mixing.

We discuss the effects of rotation in RGB stars taking into account the latest prescriptions for the transport of AM in stellar interiors and the associated mixing processes. We describe the physical inputs of our models in Sects. 3 and 4, and their effects on the angular velocity profiles and diffusion coefficients in Sect. 5. In Sect. 6 we present the results for the structural evolution and surface abundance variations of rotating low-mass Pop II stars from the ZAMS to the upper RGB. We then give a summary of our main results, and discuss them in relation to previous works in Sect. 7, and propose new investigation paths in Sect. 8.

3. Physical inputs for the evolution of rotating stars

3.1. Standard input physics

The models presented here were computed with STAREVOL V2.30, and the reader is referred to Siess et al. (2000) and Palacios et al. (2003, Paper I) for a detailed description. Let us recall the main input physics.

The nuclear reaction rates have been updated using version 5.0 of the nuclear network generator NetGen available at IAA (`http://astropc0.ulb.ac.be/Netgen`). By default the adopted rates are NACRE (Angulo et al. 1999) for charged particles, Bao et al. (2000) for neutron capture rates, Horiguchi et al. (1996) for experimental beta decay rates, and Caughlan & Fowler (1988) otherwise.

For the radiative opacities, we used the OPAL tables[3] above 8000 K (Iglesias & Rogers 1996) and the atomic and molecular opacities of Alexander & Fergusson (1994) at lower temperatures. The conductive opacities are computed from a modified version of the Iben (1975) fits to the Hubbard & Lampe (1969) tables for non-relativistic electrons and from Itoh et al. (1983) and Mitake et al. (1984) for relativistic electrons.

The equation of state is described in detail in Siess et al. (2000) and accounts for the non ideal effects due to Coulomb interactions and pressure ionisation. The standard mixing length theory is used to model convection with $\alpha_{\rm MLT} = 1.75$, and the atmosphere is treated in the gray approximation and integrated up to an optical depth $\tau \simeq 5 \times 10^{-3}$.

3.2. Transport of angular momentum

The evolution of AM and chemical species follow Zahn (1992) and Maeder & Zahn (1998). Meridional circulation and turbulence induced by the secular shear instability are the two transport mechanisms considered here. Within this framework, the transport of AM obeys an advection/diffusion equation

$$\rho \frac{{\rm d}\left(r^2\Omega\right)}{{\rm d}t} = \frac{1}{5r^2}\frac{\partial}{\partial r}\left(\rho r^4 \Omega U_r\right) + \frac{1}{r^2}\frac{\partial}{\partial r}\left(r^4 \rho \nu_{\rm v} \frac{\partial \Omega}{\partial r}\right), \quad (1)$$

where ρ, r, and Ω have their usual meaning; $\nu_{\rm v}$ is the vertical component of the turbulent viscosity associated with the shear instability; and U_r is the vertical component of the meridional circulation velocity, which, assuming shellular rotation[4], is given by:

$$U_r = \frac{P}{C_{\rm p}\rho T g[\nabla_{\rm ad} - \nabla + \varphi/\delta\nabla_\mu]} \times \left[\frac{L}{M_*}(E_\Omega + E_\mu)\right] \quad (2)$$

where $M_* = M(1 - \frac{\Omega^2}{2\pi G\rho_{\rm m}})$. There, E_Ω and E_μ depend, respectively, on the relative horizontal variation of the density,

[3] The OPAL tables used are based on a solar-scaled chemical mixture with possible enhancement of C and O, but do not include *alpha*-element enhancement.

[4] The condition of shellular rotation is satisfied when turbulence is highly anisotropic and ensures $\Omega \approx \Omega(P)$. In that case, Zahn's formalism may be applied strictly. Otherwise, it represents a first-order approximation.

$\Theta = \frac{\tilde{\rho}}{\rho} = \frac{1}{3}\frac{r^2}{g}\frac{\mathrm{d}\Omega^2}{\mathrm{d}r}$, and of the mean molecular weight, $\Lambda = \frac{\tilde{\mu}}{\mu}$. Detailed expressions for these quantities are given in Appendix A. The evolution of Λ depends on the competition between the vertical advection of a mean molecular weight gradient $\frac{\partial \ln \overline{\mu}}{\partial r}$ and its destruction by horizontal diffusion D_h (see Sect. 3.4)

$$\frac{\partial \Lambda}{\partial t} + U_r \frac{\partial \ln \overline{\mu}}{\partial r} = -\frac{6}{r^2} D_\mathrm{h} \Lambda. \tag{3}$$

This equation is obtained under the assumption that

$$\frac{D_\mathrm{v}}{\ell_\mathrm{v}^2} \ll \frac{D_\mathrm{h}}{\ell_\mathrm{h}^2}, \tag{4}$$

where D_v is the vertical turbulent diffusion coefficient (see Sect. 3.4), ℓ_v and ℓ_h are the characteristic distance scales in the vertical and horizontal directions, respectively. As in Paper I, the transport of AM is computed by solving 5 first-order differential equations (Eq. (3) + 4 equations resulting from the splitting of Eq. (1)) with a Newton-Raphson relaxation method. The upper boundary condition on Λ has, however, been modified compared to Paper I, and we used the continuity equation at the base of the CE rather than assuming $\Lambda = 0$.

The effects of μ-currents (E_μ term in Eq. (2)) are taken into consistently account from the ZAMS up to the upper RGB.

3.3. Transport of chemicals

Chaboyer & Zahn (1992) showed that the vertical advection of chemicals by large-scale circulation combined with strong horizontal diffusion produces a vertical effective diffusivity D_eff in the presence of strong anisotropic turbulence, (see Sect. 3.4). The vertical transport of a chemical species i of concentration c_i can thus be described by a pure diffusion equation:

$$\rho \frac{\mathrm{d}c_i}{\mathrm{d}t} = \underbrace{\dot{c}_i}_{\text{nuclear}} + \underbrace{\frac{1}{r^2}\frac{\partial}{\partial r}\left[r^2 \rho U_\mathrm{ip} c_i\right]}_{\text{atomic diffusion}} + \underbrace{\frac{1}{r^2}\frac{\partial}{\partial r}\left[r^2 \rho D_\mathrm{tot}\frac{\partial c_i}{\partial r}\right]}_{\text{macroscopic processes}}. \tag{5}$$

Here, U_ip is the atomic diffusion velocity of the element with respect to protons, and D_tot is the total macroscopic diffusion coefficient, and is the sum of the effective diffusion coefficient (8) and of the vertical turbulent diffusion coefficient D_v (see Sect. 3.4).

The diffusion Eq. (5) is solved for each of the 53 species considered in the code, considering $\dot{c}_i = 0$ (that is, diffusion and nucleosynthesis are decoupled). Here again, we used a Newton-Raphson method, as for the structure and AM transport equations.

3.4. Diffusion and viscosity

Let us briefly recall the various formulations used for the diffusion coefficients entering Eqs. (1), (3), and (5).

- ν_v, D_v
  As in Paper I, we assume that the secular shear instability dominates and that vertical shear eventually becomes turbulent in the radiative stellar interiors due to the low viscosity of the plasma (Zahn 1974). The development of turbulence is subject to the Reynolds criterion and sets in when

  $$\mathrm{Re} = \frac{\nu_\mathrm{v}}{\nu_\mathrm{mol} + \nu_\mathrm{rad}} > \mathrm{Re_c},$$

  where $\nu_\mathrm{rad} = \frac{4}{15}\frac{aT^4}{\kappa\rho^2}$ is the radiative viscosity, ν_mol is the molecular viscosity, and $\mathrm{Re_c} \simeq 10$ is the critical Reynolds number. The shear instability obeys the Richardson criterion, and according to the classical formulation it should set in when

  $$\frac{\mathrm{d}u}{\mathrm{d}z} > \frac{N^2}{\mathrm{Ri_c}},$$

  where $\mathrm{Ri_c} = 0.25$ is the critical Richardson number. Here, we consider rather a modified Richardson criterion to take radiative losses and/or horizontal diffusion into account as described below. Several modified criteria have been proposed; in this paper, we will compare results obtained with two of them.
  - The first criterion assumes that thermal diffusion reduces the stabilising effect of thermal stratification without affecting the chemical part. It leads to (cf. Maeder & Meynet 1996):

    $$D_\mathrm{v} = \nu_\mathrm{v} = \frac{8}{5} K_\mathrm{T} \frac{\mathrm{Ri_c}(r\mathrm{d}\Omega/\mathrm{d}r)^2 - N_\mu^2}{N_\mathrm{T}^2}, \tag{6}$$

    where $N^2 = N_\mathrm{T}^2 + N_\mu^2$ is the Brunt-Väisälä frequency and K_T the thermal diffusivity. In this paper we refer to this prescription as *MM96*.
  - The second criterion, which we used in Paper I, also considers the erosion of the chemical stratification by the large horizontal diffusion (cf. Talon & Zahn 1997):

    $$D_\mathrm{v} = \nu_\mathrm{v} = \frac{8}{5} \frac{\mathrm{Ri_c}(r\mathrm{d}\Omega/\mathrm{d}r)^2}{N_\mathrm{T}^2/(K_\mathrm{T} + D_\mathrm{h}) + N_\mu^2/D_\mathrm{h}}, \tag{7}$$

    where D_h is the horizontal turbulent viscosity. In this paper we refer to this prescription as *TZ97*.

  Let us further note that, due to the lack of a better prescription, we assume $D_\mathrm{v} = \nu_\mathrm{v}$.
- D_eff.
  The effective diffusion coefficient appears solely in the transport equation of chemicals. In the approximation of highly anisotropic turbulence, this is the diffusive representation of the effects of meridional circulation (Chaboyer & Zahn 1992), and can be written as follows:

  $$D_\mathrm{eff} = \frac{|rU_r|^2}{30 D_\mathrm{h}}. \tag{8}$$

- ν_h, D_h.
  The vertical turbulent diffusion coefficient D_v, as well as the effective diffusion coefficient D_eff, depends on the horizontal component of the turbulent diffusivity D_h. No description of this diffusivity can be drawn from first principles, and its expression has to be parametrised. Assuming that the differential rotation on an isobar is small compared to unity, Zahn (1992) first proposed the following expression for ν_h:

  $$\nu_\mathrm{h} = \frac{r}{C_\mathrm{h}} \left| \frac{1}{3\rho r}\frac{\mathrm{d}(\rho r^2 U)}{\mathrm{d}r} - \frac{U}{2}\frac{\mathrm{d}\ln r^2\Omega}{\mathrm{d}\ln r} \right| \equiv \frac{r}{C_\mathrm{h}} \left| 2V - \alpha U \right|, \tag{9}$$

  where C_h is a free parameter of order 1, which we used in our Paper I; $V = \frac{1}{6\rho r}\frac{\mathrm{d}}{\mathrm{d}r}\left(\rho r^2 U\right)$ is the horizontal component of the meridional velocity; and $\alpha = \frac{1}{2}\frac{\mathrm{d}\ln r^2\bar{\Omega}}{\mathrm{d}\ln r}$. Meanwhile, some improvements have been achieved and more realistic prescriptions for the horizontal shear turbulent diffusivity, including a dependence on the rotation rate, derived by Maeder (2003) and Mathis et al. (2004):

  $$\nu_\mathrm{h} = \chi^{\frac{1}{n}}\, r \left(r\, \bar{\Omega}(r)\, V^k \left[2V - \alpha U\right]\right)^{\frac{1}{n}}, \tag{10}$$

where $(\chi; n; k) = (\frac{3}{400m\pi}; 3; 1)$ in Maeder's expression (with $m = 1$, 3 or 5), and $(1.6 \times 10^{-6}; 2; 0)$ in Mathis et al. (2004). In Maeder (2003), the horizontal turbulent viscosity ν_h is derived from a comparison between the dissipation rate of turbulent energy by meridional circulation and the viscous dissipation rate, while it is derived in Mathis et al. (2004) from Couette-Taylor laboratory experiments (see Richard & Zahn 1999).

The horizontal turbulent diffusion coefficient D_h obtained by Eq. (10) is larger than the one derived from expression Eq. (9) and is more consistent with the shellular rotation hypothesis. In the following, we compare results obtained with these two prescriptions, which we refer to as Zahn92 and *MPZ04* (see Table 1).

Table 1. Rotation input physics of the models. D_h: MPZ04 refers to Mathis et al. (2004) whereas Zahn92 refers to Zahn (1992). D_v: TZ97 refers to Talon & Zahn (1997) and MM96 refers to Maeder & Meynet (1996).

Model	CE rotation law	υ_{ZAMS} km s^{-1}	Braking	D_h	μ-currents	D_v
M0	—	0	—	—	—	—
M1	**$\Omega(r)$ = const.**	**5**	**no**	**MPZ04**	yes	TZ97
M2	$j(r)$ = const.	5	no	MPZ04	yes	TZ97
M3	$j(r)$ = const.	5	no	MPZ04	no	TZ97
M4	$j(r)$ = const.	5	no	MPZ04	yes	MM96
M5	$j(r)$ = const.	5	no	Zahn92	yes	TZ97
M6	$j(r)$ = const.	110	yes	MPZ04	yes	TZ97

3.5. Rotation law in the convective envelope

The formalism developed by Zahn (1992) describes the transport of AM in radiative zones, and the rotation profile in the CE is defined by an upper boundary condition. Its choice is, however, of prime importance since it determines the flux of angular momentum between these two regions.

In the case of RGB stars, this will play an essential role, as discussed in Sect. 5.1.

The interaction between rotation and convection is a long-standing and not fully understood problem, and despite the development of 3D numerical simulations (Ballot et al. 2004; Browning et al. 2004), the rotation profile within deep convective envelopes remains unknown. As already suggested by SM79, we may consider two limiting cases for the CE rotation law,

1. *Uniform angular velocity (solid body rotation)*
   This hypothesis has generally been assumed when modelling the evolution of rotating stars (Endal & Sofia 1978; Talon et al. 1997; Meynet & Maeder 2000; Paper I). It is also the rotation regime obtained when describing AM transport in the CE by a diffusion equation using the diffusion coefficient derived from the MLT theory (Heger et al. 2000). Imposing solid body rotation in the CE is thus equivalent to assuming that the meridional currents are inhibited in the presence of convection and that the turbulent viscosity associated with convection is large enough to allow for instantaneous homogenisation of the angular velocity profile $\Omega(r)$, as is the case for chemicals (Endal & Sofia 1976). This condition is also motivated by observations of the solar convection zone (the sole star for which we have such information at present), where *radial* differential rotation is minute (Kosovichev et al. 1997).
2. *Uniform specific angular momentum (differential rotation)*
   Already in the early 70's, Tayler (1973) addressed the effects of rotation in stellar convective zones and came to the conclusion that meridional currents could develop and alter the rotation law in stellar convective regions. With caution, he suggested that "*it is possible that the asymptotic state [of rotation in a convective zone] is closer to one of uniform angular momentum than uniform angular velocity*". Some years later, Sweigart & Mengel (1979) proposed that rotation-induced mixing by meridional circulation could explain both the CNO abundance anomalies in RGB stars and the slow rotation rates observed in MS low-mass stars provided the radiative interior conserves its angular momentum during the first ascent of the giant branch, and the CE has *constant* ($\mathrm{d}j_{CE}/\mathrm{d}t = 0$) and *uniform* ($\mathrm{d}j_{CE}/\mathrm{d}r$ = const.) specific angular momentum. More recently, Denissenkov & Tout (2000) investigated both possibilities for rotation in the CE of a low-mass RGB star and concluded in favour of uniform and constant specific angular momentum in the CE. Investigating the rotation rates on horizontal branch (HB) stars of globular clusters, Sills & Pinsonneault (2000) show that slow rotation on MS stars and $\upsilon \sin i$ up to 40 km s^{-1} on the HB indicate that a non-negligible amount of AM is preserved in the stellar interior between the MS turn-off and the HB. They propose that this could be achieved assuming uniform specific angular momentum in the CE during the RGB phase, again a conclusion similar to that drawn by SM79 and more recently, by Chanamé et al. (2004a,b).
   These studies indicate that the condition of differential rotation in the CE (i.e. $j_{CE}(r) = \frac{2}{3}r^2\Omega(r)$ = const.) could be a key ingredient in deriving a consistent history of the AM evolution in low-mass stars, as well as in producing a high degree of mixing in the RGB interiors needed to explain part of the abundance anomalies observed at this phase.

4. Numerical simulations

We model a typical metal-poor globular cluster RGB star with initial mass $M = 0.85\ M_\odot$, initial helium content $Y_{ini} = 0.248$, and [Fe/H] = −1.57 which corresponds to the metallicity of M 13 stars (Sneden et al. 2004). We take the α-enrichment expected at such metallicities into account, with [O/Fe] = [Ne/Fe] = [Mg/Fe] = +0.3 dex, and account for the odd-even effect on sodium, with [Na/Fe] = −0.3 dex. The initial ratio for the magnesium isotopes is ^{24}Mg:^{25}Mg:^{26}Mg = 87.5:6:6.5, and is similar to the values determined by Yong et al. (2003) for the stars with the lowest ^{25}Mg and ^{26}Mg in NGC 6752, a globular cluster with [Fe/H] ≈ −1.6. The mass fractions of the other elements are in solar system proportion and are scaled for their sum to be equal to unity. This corresponds to a metallicity of $Z = 8 \times 10^{-4}$.

Mass loss is included from the ZAMS on in all our models. We use the empirical Reimers (1975) formula with a metallicity scaling:

$$\dot{M} = -3.98 \times 10^{-13} \eta \frac{LR}{M} \sqrt{\frac{Z}{Z_\odot}}\ M_\odot\ \mathrm{yr}^{-1} \qquad (11)$$

with $\eta = 0.5$. At each time step, the associated AM losses are taken into account and the adjusted total AM is conserved when applying rotational transport.

All models are computed assuming uniform angular velocity in the CE during the MS as indicated by the solar case. When

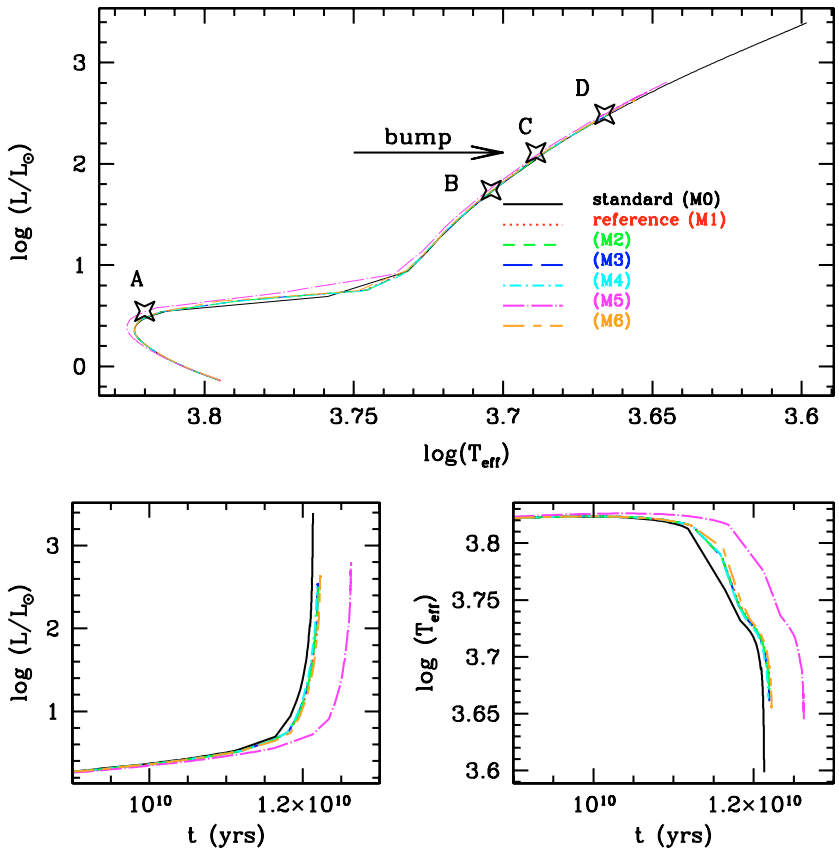

Fig. 1. *Upper panel*: Hertzsprung-Russell diagram for the different test models presented. All sequences start with $M_{\rm ZAMS} = 0.85\ M_\odot$, [Fe/H] = −1.57. Evolutionary tracks for models M1 and M3 are superimposed. Open symbols labelled A, B, C and D correspond to the turn-off, the end of the 1st DUP, the *bump* and $L = 310\ L_\odot$ respectively. *Lower panels*: evolution of luminosity (*left*) and effective temperature (*right*) as a function of time beyond the turn-off.

considered, the hypothesis of uniform specific angular momentum in the CE is applied beyond the turn-off, i.e. when the convective envelope begins to deepen. All models were computed with uniform angular velocity in the CE during the MS phase. Braking, if applied, begins at the ZAMS following a Kawaler (1988) law calibrated in order to lead to equatorial rotational velocity of $\upsilon \approx 10\,{\rm km\,s^{-1}}$ when they reach the Hyades age (this occurs for $T_{\rm eff} \approx 6300$ K) early on the main sequence. This velocity is typical of cool stars in the Hyades. We compare two different rotational histories, namely models that were already slow rotators on the ZAMS and models with the initially higher velocity typical of ZAMS Pop I stars, but that experience magnetic braking in their early evolution, as expected from solar-type stars. This braking results in similar surface velocities half-way on the main sequence (when $X_{\rm c} \approx 0.5$) for initially fast and slow rotators. Considering their important role in shaping the rotation profile (see Paper I), the so-called μ-currents (E_μ term in Eq. (2)) are taken into account in all our rotating models, except for M3. In all cases the initial rotation profile at the ZAMS is defined by $\Omega(r) = \upsilon_{\rm ini}/R_\star = \text{const.}\ \ \forall\ \ r$.

We finally underline that Eq. (1) is solved in all its complexity for all the rotating models presented here from the ZAMS up to the upper RGB.

Table 1 lists the characteristics of the models that we have computed using different prescriptions for the input physics. For our reference model (M1), we consider the following set of parameters/physical ingredients: uniform angular velocity in the convective regions at all times, initial surface velocity of $5\,{\rm km\,s^{-1}}$ on the ZAMS with no braking applied, the Mathis et al. (2004; Eq. (10)) and Talon & Zahn (1997; Eq. (7)) prescriptions for the horizontal $\nu_{\rm h}$, and vertical $\nu_{\rm v}$ turbulent diffusion coefficients, respectively.

Figure 1 presents the Hertzsprung-Russell diagram and the evolution of the surface luminosity and temperature for the models computed. It will be discussed in more detail in Sect. 6.1. The evolutionary points on which we focus in the following sections are marked on the evolutionary path and correspond to the turn-off (A), the end of the first DUP (B), the bump (C), and $L = 310\ L_\odot$ (D).

5. Testing the physics of rotation

In this section, we analyse the impact of the different physical inputs included in the models presented in Table 1.

5.1. Rotation in the convective envelope

In Sect. 3.5 we mentioned the uncertainty regarding the rotation law in the convective envelope of a giant star. Previous studies also provide some hints that the evolution of the AM (and chemicals) distribution within the radiative interior might strongly depend on the rotation regime at the base of the convective envelope. This aspect can be studied by comparing models M1 and M2, which differ solely by the applied rotation law in the CE beyond the turn-off.

Profiles of the angular velocity Ω, of the horizontal density fluctuations $\theta\ (=\frac{\Theta}{\Omega} = \frac{1}{3}\frac{r^2}{g}\partial\Omega/\partial r)$, and of the specific angular momentum j at four different evolutionary stages for models M1, M2, and M6 are presented in Figs. 2 and 3. In Fig. 2, as well as in several other figures in this paper, quantities are plotted against δM instead of M_r. The variable δM is a relative mass

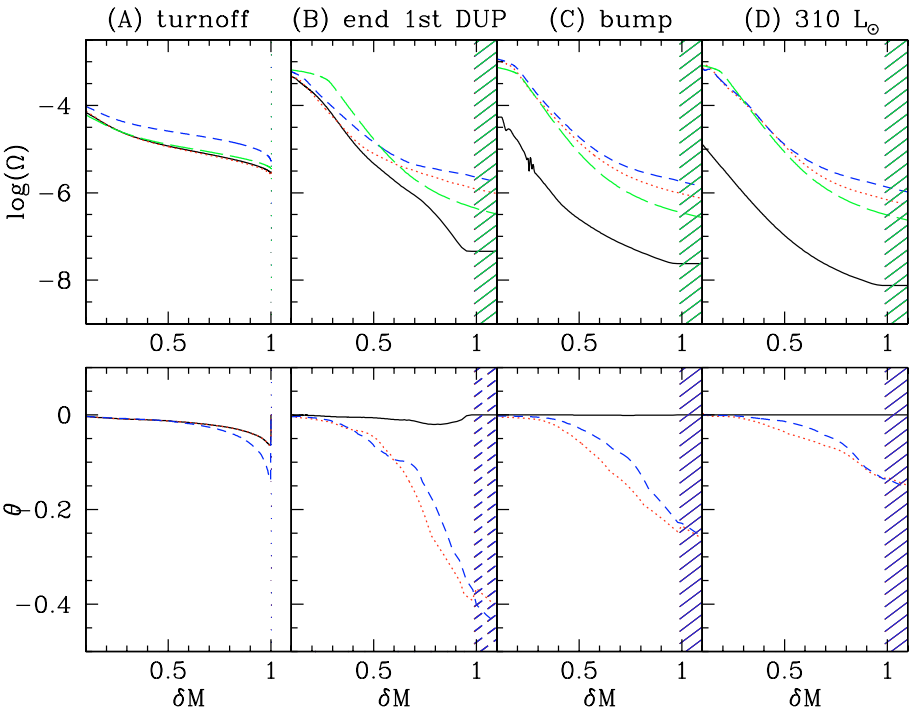

Fig. 2. Angular velocity Ω and horizontal density fluctuations $\theta \propto \partial\Omega/\partial r$ inside models M1 (solid lines), M2 (dotted lines), and M6 (dashed lines) at the four evolutionary points top-labelled on the graph and reported in Fig. 1. Both Ω and θ are plotted against the scaled mass coordinate δM, which allows a blow-up of the region of interest ($\delta M = 0$ at the base of the HBS and $\delta M = 1$ at the base of the CE). The long dashed lines on the *upper panels* represent the Ω profiles that one gets when the angular momentum evolution in model M2 only results from the structural readjustments beyond the turn-off (i.e. no AM transport).

coordinate allowing for a blow-up of the radiative region above the HBS, and is defined as

$$\delta M = \frac{M_r - M_{\rm HBS}}{M_{\rm BCE} - M_{\rm HBS}}, \qquad (12)$$

where δM is equal to 1 at the base of the convective envelope and 0 at the base of the HBS (where $X = 10^{-7}$). In our models, the nuclear reactions typically occur between $\delta M = 0.2$ and $\delta M = 0.5$, a large mean molecular gradient being associated with the layers of maximum energy production at $\delta M = 0.2$

By assumption, the rotational evolution is identical in models M1 and M2 up to the turn-off. Beyond, the evolution of the AM distribution is dominated by structural readjustments of the star becoming a giant. The degree of differential rotation in the radiative zone globally increases with time, leading to a rapidly rotating core and a slowly rotating surface (Ω rises by 3 to 4 orders of magnitude between the base of the CE and the edge of the degenerate He core in both models).

At the turn-off, the base of the CE rotates at the same velocity in models M1 and M2. As the star crosses the Hertzsprung gap and approaches the Hayashi line on its way to the red giant branch, the core contracts, while the outer layers expand and are thus efficiently slowed down. For model M1, the velocity of the inner shells of the envelope also decreases substantially because of the solid-body rotation of the CE ($\mathrm{d}\Omega_{\rm CE}/\mathrm{d}r = 0$), and the AM attached to the convective envelope concentrates in the outer layers. At the end of the 1st DUP, the angular velocity at the base of the CE, $\Omega_{\rm BCE}$, decreases by a factor of 65. When the CE withdraws in mass, it leaves behind radiative shells with low specific angular momentum that rotate slowly. The resulting differential rotation rate is low in this region as shown in the θ and Ω profiles.

For model M2, the surface layers slow down during the 1st DUP, but the uniformity of the specific angular momentum prevents the shells of the inner CE from decelerating abruptly and ensures the concentration of AM in this denser region. At the end of the 1st DUP, $\Omega_{\rm BCE}$ has only decreased by a factor of 3. As the CE withdraws in mass, its deeper shells retaining the larger part of the CE angular momentum fall back into the underlying radiative zone, where they conserve their large angular velocity and strong differential rotation.

Figure 3 shows that after the completion of the 1st DUP, the assumption of uniform specific angular momentum within the CE also translates into a quasi-constancy of the level of specific angular momentum in this region (dotted and dashed lines in panels (B), (C), and (D)). This is a natural expectation since the convective envelope of a red giant represents more than 80% of the stellar radius and retains most of the angular momentum. The assumption of the *constancy* of $j_{\rm CE}$ (e.g. no variation with time) under a regime of uniform specific angular momentum remains, however, an approximation since transfer of AM occurs between the interior and the envelope. Our models indicate that the specific angular momentum in the envelope indeed increases slightly with time.

The difference of the rotation profiles encountered in models M1 and M2 below the CE affects the diffusion coefficients, in particular $D_{\rm v}$, which scales as $(r\mathrm{d}\Omega/\mathrm{d}r)^2$. Figures 4 and 5 present the profiles of the diffusion coefficients entering the transport equations of AM and chemicals (Eqs. (1) and (5)) at the end of the 1st DUP, at the *bump*, and at $L = 310\ L_\odot$ for models M1 and M2, respectively. One may notice that $D_{\rm h}$ is much larger everywhere than $D_{\rm v}$ (see also Figs. 6, 8 and 9). This validates the shellular rotation hypothesis.

– *Model M1*
At the end of the 1st DUP (left panel in Fig. 4), differential rotation is negligible below the CE in the region between $\delta M \simeq 0.5$ and $\delta M = 0.91$. There, the vertical turbulent viscosity is smaller than its critical value given by $\nu_{v,\rm crit} = \mathrm{Re_c}\nu_{\rm rad} \simeq 3000$, and turbulence does not develop. *The low rate of differential rotation quenches the turbulent transport and creates a gap that disconnects the CE from the regions where nucleosynthesis occurs.* Below $\delta M \simeq 0.5$ the differential rotation is larger and the shear turbulence dominates the transport down to the region ($\delta M \approx 0.1$) where both meridional circulation and shear turbulence are very efficiently hindered by the high mean molecular weight barrier

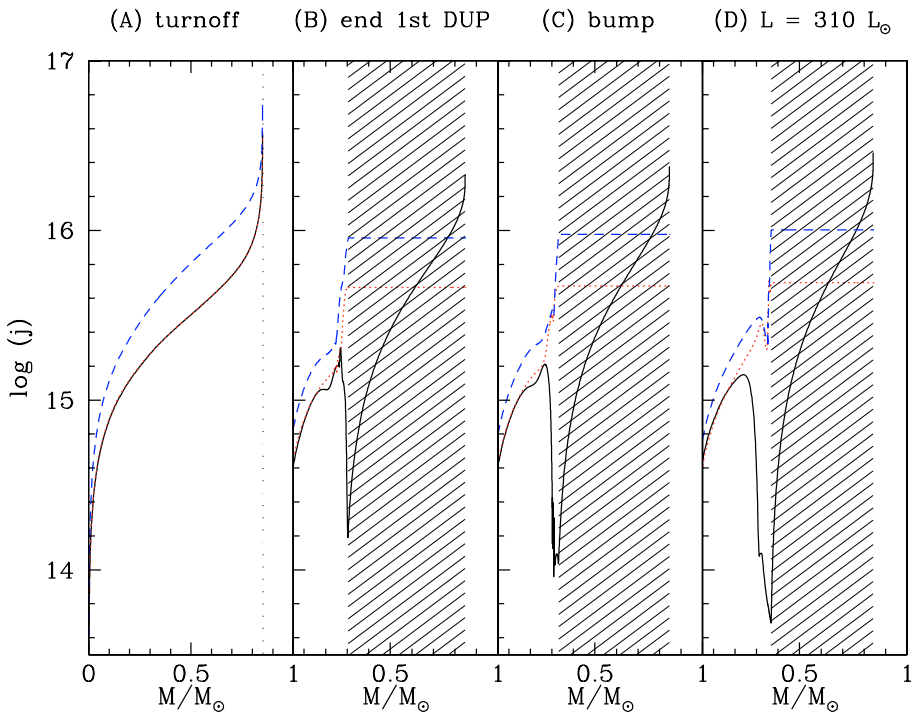

Fig. 3. Profile of the logarithm of the specific angular momentum $\log(j)$ inside models M1 (solid lines), M2 (dotted lines), and M6 (dashed lines) at the four evolutionary points top-labelled on the graph and reported in Fig. 1, as a function of the internal mass coordinate M_r in units of $M_\odot$.

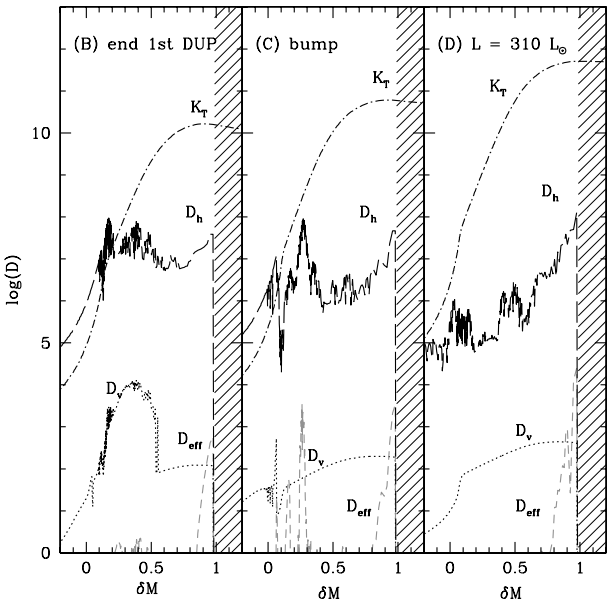

Fig. 4. Profiles of the different diffusion coefficients at the end of the first dredge-up (*left panel*) and at the *bump* (*right panel*) for our reference model (M1 in Table 1).

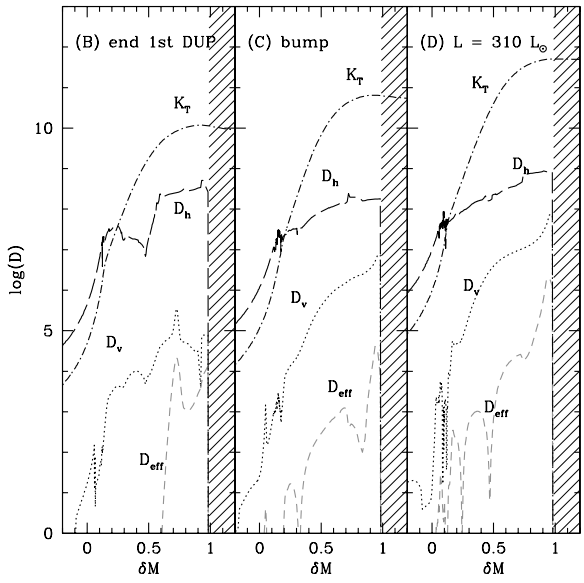

Fig. 5. Same as Fig. 4 for M2 in Table 1. M2 only differs from M1 by the adopted differential rotation law in the convective envelope.

associated with the hydrogen burning (see upper panels of Fig. 10). At the *bump* and beyond, shear-induced turbulence does not develop and the effective diffusion coefficient remains negligible below $\delta M \simeq 0.85$, so that no modification of the surface abundance pattern by rotational mixing should be expected beyond this point (see Sect. 6.2).

– *Model M2*

When assuming uniform specific angular momentum in the CE, the picture is very different (Fig. 5). The larger differential rotation rate allows the shear flow to become turbulent almost everywhere between the base of the CE and the HBS. Shear turbulence dominates the transport of chemicals across the entire radiative zone, the effective diffusion coefficient associated with meridional circulation being always much smaller in the whole radiative region. Anticipating the results of Sect. 6.2, we can already see from Fig. 10 that $D_{\rm tot}$ does not rise above 10^5 cm^2 s^{-1} in the outer HBS (around $\delta M = 0.2$–0.3) even at the *bump*, which is much lower than the parametric "canonical mixing rate" of 4×10^8 cm^2 s^{-1} deduced from observational constraints (Denissenkov & VandenBerg 2003).

The profile of $D_{\rm eff}$ in Fig. 5 appears to be quite ragged below $\delta M \simeq 0.5$, in particular in panel (D). Each of the bumps in this region is associated with an inversion of the meridional circulation velocity, which can be positive or negative. Although the meridional circulation can actually present various cells, these

particular features are due to numerical instabilities occurring in the regions where the mean molecular weight gradients are non-negligible. When the effects of μ-currents are included (terms depending on μ or Λ in Eq. (2)), the numerical system is highly non-linear and may be sensitive to numerical parameters such as the spatial and temporal resolutions.

The global amplitude of $D_{\rm eff}$ (and $D_{\rm v}$) in these regions of large μ-gradients, together with the decrease in the diffusion coefficients in the nuclearly active shells, are, however, robust results. Just below the CE, the first bump in the $D_{\rm eff}$ profile is also a robust feature, associated with the Gratton-Öpik meridional circulation cell. These remarks apply to all our models.

5.2. Impact of the ZAMS rotation velocity

We investigated the impact of the initial rotational velocity by considering an originally slow (model M2) and a fast rotator (model M6) on the ZAMS, without changing any of the other physical parameters. We applied the same treatment to model M6 as to Pop I stars (see Paper I), namely a strong magnetic braking according to the Kawaler (1988) prescription so as to get a surface equatorial velocity lower than 10 km s^{-1} before the central hydrogen mass fractions gets lower than 0.5. At the turn-off, the surface velocities of models M6 and M2 are thus quite similar (see Table 3).

This section is meant to determine whether this strong braking, which triggers strong turbulence in the radiative zone during the main sequence, has an effect on the angular momentum distribution and on the diffusion coefficients beyond the turn-off. In the present study, we did not investigate the case of fast rotators at the turn-off, this configuration being ruled out by the velocities available from observations of low-mass turn-off stars in globular clusters (Lucatello & Gratton 2003).

Figure 2 presents the degree of differential rotation (θ profiles) and the angular velocity inside models M2 and M6 at different evolutionary points. Model M6 rotates globally faster than model M2 at the turn-off, and this difference is maintained during the evolution. Indeed, although model M6 undergoes a very efficient braking on the early MS, it is only braked down to 5.7 km s^{-1} at the turn-off, compared to 3.88 km s^{-1} in model M2. In spite of these different surface rotation rates, the profiles of Ω and θ are quite similar in the radiative zone of these models during the RGB phase (Fig. 3). Consequently, the turbulent diffusion coefficients (see Eq. (7)) are not very different during the RGB phase, as can be seen in Figs. 5, 6, and 10.

This comparison shows that the structural readjustments (induced the 1st DUP) efficiently redistribute the AM throughout the star beyond the turn-off. The resulting rotation profile after the completion of the 1st DUP is almost solely determined by the star's total angular momentum at the turn-off and by the CE rotation law.

5.3. The μ-currents and horizontal turbulence

The mean molecular weight affects the transport of chemicals via its gradient ∇_μ and its relative horizontal variation Λ (see Eqs. (2) and (A.2)). The μ-gradients inhibit the efficiency of meridional circulation, and μ-currents are inhibited by strong horizontal turbulence. In Paper I we emphasised the importance of these terms in establishing the differential rotation profile during the MS for Pop I stars.

In order to better assess the role of μ-currents in Pop II stars and to determine their sensitivity to the horizontal turbulence

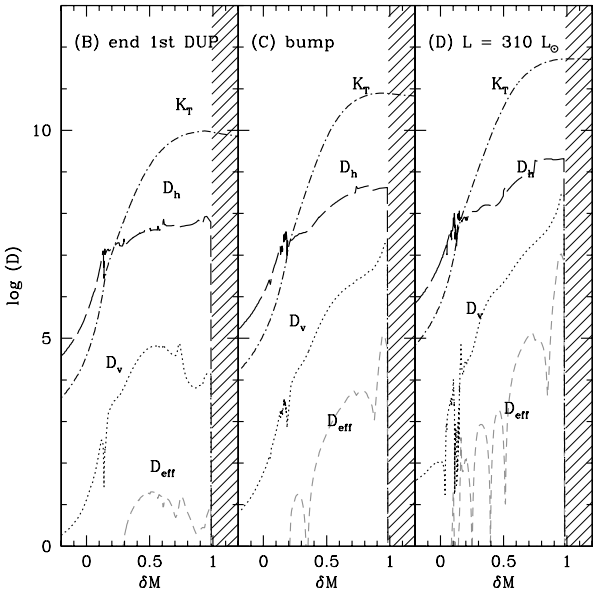

Fig. 6. Same as Fig. 4 for M6. In this model, $\upsilon_{\rm ZAMS}$ = 110 km s^{-1} and after efficient braking through according to a Kawaler law, $\upsilon_{\rm TO}$ = 6.4 km s^{-1}. Uniform specific angular momentum was assumed in the CE.

Table 2. Input parameters for the models discussed in Sect. 5.3. Some of the models appearing in this table are also listed in Table 1. Models Ma, Mb, Mc, Md, and Mh have only been computed up to the turn-off. In all models, solid-body rotation in the CE has been assumed, and $D_{\rm v}$ is given by TZ97.

Model	$\upsilon_{\rm ZAMS}$ km s^{-1}	Braking	$D_{\rm h}$	μ-currents	line style in Fig. 7
Ma	110	yes	MPZ04	no	solid
Mb	110	yes	MPZ04	yes	dotted
Mc	110	yes	Zahn92	yes	short-dashed
Md	110	yes	Zahn92	no	long-dashed
M3	5	no	MPZ04	no	solid
M2	5	no	MPZ04	yes	dotted
M5	5	no	Zahn92	yes	short-dashed
Mh	5	no	Zahn92	no	long-dashed

description, we computed a series of models for which we alternately use the Zahn92 and the MPZ04 prescriptions for $D_{\rm h}$, assuming both $E_\mu = 0$ and $E_\mu \neq 0$, and then $\upsilon_{\rm ZAMS}$ = 5 km s^{-1} and $\upsilon_{\rm ZAMS}$ = 110 km s^{-1}, for each case. The properties of these models are summarised in Table 2.

Main sequence

Let us first comment on the MS evolution. The profiles of Ω, U_r, and $D_{\rm tot}$ are displayed in Fig. 7 at three different times on the MS (see Table 2 for a detailed description of each curve).

Slow rotators on the ZAMS (Fig. 7, left panels).

Their slow rotation, together with the negligible structural readjustments occurring during the MS, does not favour any mechanism able to trigger steep rotation profiles. As a result, the transport of both angular momentum and chemicals by rotation-induced processes is inefficient. This is independent of the choice for the $D_{\rm h}$ prescription and of the introduction or not of the μ-currents. The Ω-profile, as well as the total diffusion

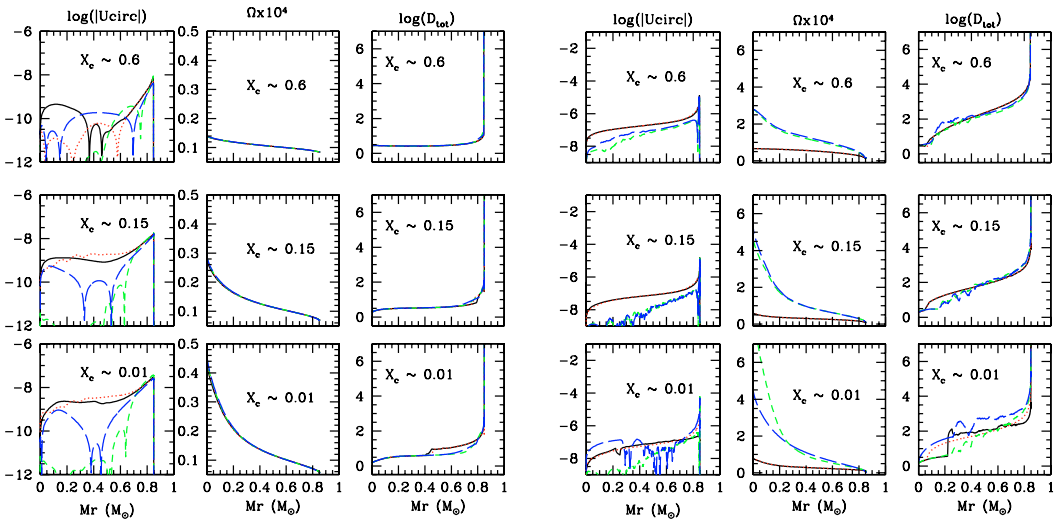

Fig. 7. Profiles of the vertical component of the meridional circulation velocity U_r, angular velocity Ω, and total diffusion coefficient $D_{\rm tot}$ inside 0.85 $M_\odot$, [Fe/H] = −1.57 models at three stages of their evolution (as indicated by their central H content $X_{\rm c}$: $X_{\rm c} = 0.6 \Leftrightarrow t \approx 2$ Gyr, $X_{\rm c} = 0.15 \Leftrightarrow t \approx 8$ Gyr, and $X_{\rm c} = 0.01 \Leftrightarrow t \approx 10$ Gyr). *First 3 columns on the left*: profiles for models that are slow rotators on the ZAMS ($\upsilon_{\rm ZAMS} = 5$ km s^{-1}) and undergo no braking; *last 3 columns on the right*: profiles of initially fast rotating models on the ZAMS ($\upsilon_{\rm ZAMS} = 110$ km s^{-1}) that undergo strong magnetic braking during their early MS evolution. Here, solid and dashed lines are superimposed and indistinguishable from one another. Details on input parameters are given in Table 2.

coefficient for chemicals, is similar in all cases. The μ-gradients in the radiative interior are small, which makes the effects of μ-currents negligible during the MS.

Fast rotators on the ZAMS (Fig. 7, right panels).

Turning now to the fast rotators on the ZAMS, the strong braking at the beginning of the MS allows the build-up of steeper Ω-gradients, and shear-turbulence can develop across the radiative zone already during the main sequence. This leads to efficient transport of both angular momentum and chemicals, similar to what is obtained in their Pop I counterparts. The μ-gradients are larger in this case than for slow rotators, and we can expect μ-currents to have the same effects on the rotation profile as those observed in the Pop I stars. It is actually the case when considering the *Zahn92* prescription for $D_{\rm h}$ that was used in Paper I. As shown in Fig. 7, when the μ-currents are taken into account ($E_\mu \neq 0$), the degree of differential rotation reached near the end of the MS is substantially higher than when these terms are neglected. The μ-currents also limit the extent of the shear unstable region at the centre, whereas when $E_\mu = 0$, turbulence is free to develop across the entire radiative interior (third column, Fig. 7).

Using the MPZ04 for $D_{\rm h}$ leads to a different conclusion. This prescription produces much higher values for the horizontal turbulence $D_{\rm h}$ than the former one. As the μ-currents (E_μ term in Eq. (2); see also Eq. (A.2) in Appendix) are generated by the horizontal variation of the mean molecular weight, they are much reduced by this choice. In the case we are considering, they are reduced to an insignificant level; e.g. they remain small compared to the Ω-currents (term E_Ω in Eq. (2); see also Eq. (A.1)) and affect neither the rotation profile nor the meridional circulation velocity.

In short, the μ-currents on the MS have negligible effects on Pop II low-mass stars that are slow rotators, independent of the prescription used for $D_{\rm h}$. This is due exclusively to the slow rotation. On the other hand, the μ-currents may affect the building of the rotation profile during the MS evolution of low-mass Pop II stars undergoing strong magnetic braking if the horizontal turbulence is not too strong to prevent any significant variation of the mean molecular weight to develop.

Red giant branch

Comparing model M2 with models M3 and M5 provides respective clues into the effects of the μ-currents (M2 versus M3) and the horizontal turbulence description (M2 versus M5) on the transport of chemicals beyond the turn-off. Figure 10 presents the total diffusion coefficients for the chemicals in all our rotating models at evolutionary points (B), (C), and (D). The total diffusion coefficient $D_{\rm tot}$ in models M2, M3, and M5 is essentially the same at the different evolutionary points presented. This indicates that μ-currents do not affect the transport of chemicals on the RGB. On the other hand, the choice of the prescription for horizontal turbulence has little effect on $D_{\rm tot}$. This is due to the fact that $D_{\rm h}$ essentially affects the effective coefficient $D_{\rm eff}$, which is much smaller than $D_{\rm v}$ after the 1st DUP in case Zahn92 is used, and remains small for MPZ04. Let us add that, in general, $D_{\rm h,MPZ04} > D_{\rm h,Zahn92}$ and that for $D_{\rm h,Zahn92}$, the shellular rotation hypothesis (i.e. $D_{\rm h} \gg D_{\rm v}$) is violated in some regions (see panel (D) Fig. 8).

5.4. Vertical turbulent diffusion coefficient

In order to compare our results with the calculations of Denissenkov & Tout (2000), we also computed a model (M4) using the MM96 prescription for $\nu_{\rm v}$ (Eq. (6)). The main differences between this criterion and the one derived by Talon & Zahn (1997) were already explained in Sect. 3.4. In Fig. 9 we present the diffusion coefficients for model M4 at the end of the 1st DUP at the *bump* and at $L \simeq 310\ L_\odot$. Unlike models M2, M3, M5, and M6, for which we also assumed uniform specific angular momentum in the CE beyond the turn-off, by the end of the 1st DUP, the shear instability has not developed between the base of the CE and the edge of the HBS in model M4. Indeed, Eq. (6) shows that the shear must be larger than N^2_μ for the

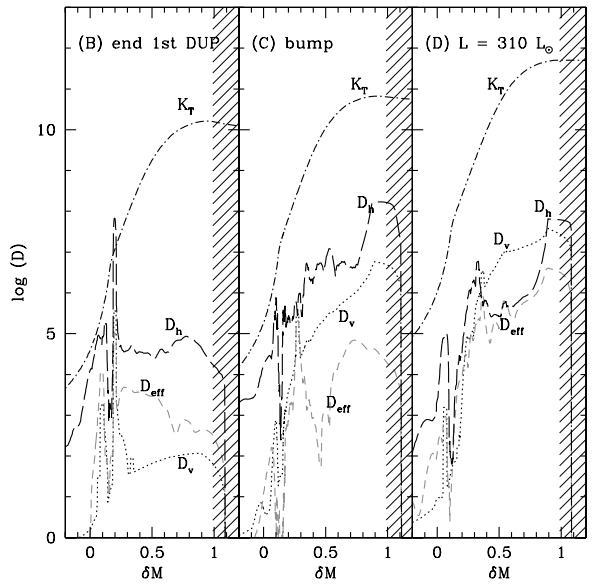

Fig. 8. Same as Fig. 4 for M5. This model is similar to M2 but was computed using the Zahn (1992) expression for $D_{\rm h}$.

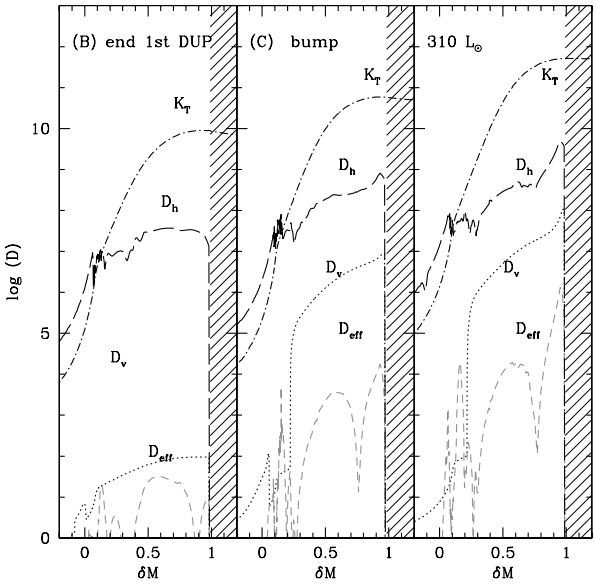

Fig. 9. Same as Fig. 4 for M4. This model is similar to M2 except that the prescription for the vertical turbulent diffusion coefficient is that of Maeder & Meynet (1996).

instability to develop. In the case of giants, it is only after completion of the 1st DUP, where the retreating CE leaves a chemically homogeneous region ($N^2_\mu = 0$), that the shear instability may set in. However the CE remains disconnected from the nucleosynthesis regions until the large μ-barrier left by the DUP is erased at the *bump*. This justifies the assumption of Denissenkov & Tout (2000) that considers rotational transport of chemicals only from the *bump* on.

However, Meynet & Maeder (1997) show that using this strong criterion prevents mixing from occurring in massive, fast rotating stars, contradicting with observational evidence. The same conclusion as reached by Talon et al. (1997) motivated the authors to introduce the erosion of the μ-gradient by horizontal turbulence. For the same reason, Maeder (1997) also developed a modified shear criterion to reduce the efficiency of mean molecular weight gradients.

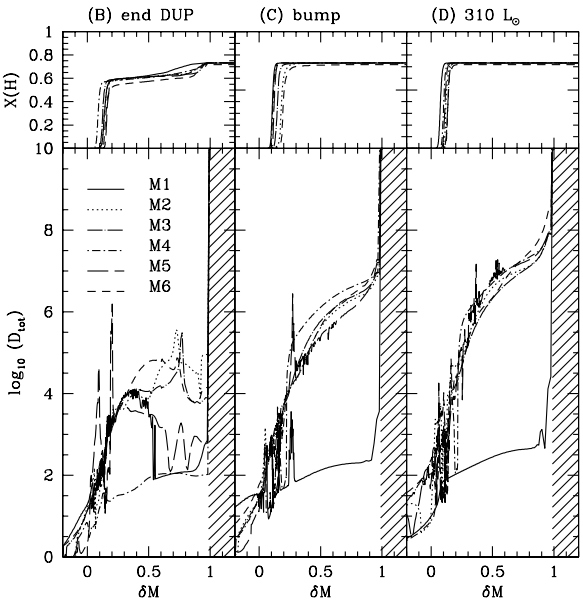

Fig. 10. *Lower panels*: total diffusion coefficient for several models (line encoding is given in the figure) as a function of the reduced mass coordinate δM at the end of the first dredge-up and at the *bump*. *Upper panels*: hydrogen mass fraction profiles in the same models.

In the same framework (i.e. study of transport associated with meridional circulation and shear turbulence) and in the absence of strong observational evidence, it is not justified to change these prescriptions for the particular case of low-mass RGB stars. It was SM79 who first suggested that prior to the *bump*, mixing should be hindered by the μ-barrier left at the end of the 1st DUP and that surface abundance variations should not be expected before this evolutionary point. We show, however, in the following that a mixing process eroding the μ-gradient does not necessarily alter the surface abundance pattern prior to the *bump*.

5.5. Dominant process for the transport of angular momentum and chemicals

In the framework of this paper, we consider two transport processes, namely meridional circulation and turbulence induced by the secular shear instability. While shear-induced turbulence is always described as a diffusive process, meridional circulation appears as an advective process for AM and as a diffusive process for the chemical species (Eqs. (1) and (5), respectively). The relative importance of these processes can thus be different depending on whether we consider AM or elements transport.

In the case of chemical species, Figs. 4–6 and 8, 9 indicate clearly that shear-induced turbulence is the dominant transport process beyond the completion of the 1st DUP when uniform specific angular momentum is assumed in the envelope. The exception is model M5, where meridional circulation is large and still dominates the transport of chemicals at the end of the 1st DUP (Fig. 8), due to the lower efficiency of the horizontal shear turbulence ($D_{\rm h} = D_{\rm h,Zahn92}$). Latter on the RGB, however, turbulence recovers the upper hand in this model, too. For model M1, shear-induced turbulence cannot be triggered in the radiative zone after the 1st DUP, and meridional circulation accounts for the transport for chemicals. The value of $D_{\rm eff}$ always remains, however, smaller that the molecular viscosity $\nu_{\rm mol}$.

In order to estimate the efficiency of the two processes responsible for the AM transport, we compared their relative characteristic timescales. The characteristic timescales for AM transport by meridional circulation and by shear-induced turbulence over a distance Δr can be estimated as $\tau_U \sim \frac{\Delta r}{U_r}$ and $\tau_\nu \sim \frac{(\Delta r)^2 \Omega}{D_v \Delta\Omega}$, respectively. $\tau_U \ll \tau_\nu$ at the end of the 1st DUP for all models but model M1. This situation is subsequently modified as shells with a large angular momentum are incorporated from the inner CE into the radiative interior. From the *bump* on, the efficiency of turbulence thus becomes similar to that of meridional circulation, with $\tau_\nu \simeq \tau_U \sim 10^5$ yr. For model M1, $\tau_\nu \simeq \tau_U \simeq 10^7$ yr from $\delta M \sim 0.1$ to 0.8 at all times (evolutionary points (B), (C), and (D)). In the region just below the CE, for $\delta M \in [0.8; 1]$, the degree of differential rotation is very small (see Fig. 2) so that the timescale for AM transport by turbulence is of the order of 10 Gyr, and meridional circulation dominates.

Between the turn-off and the completion of the 1st DUP, meridional circulation dominates the transport of AM in all our models, while the chemical species are mainly transported through turbulence. Beyond the 1st DUP, chemicals are transported via shear-induced turbulence, while the AM essentially evolves due to structural readjustments. Indeed at this phase, the advective (meridional circulation) and the diffusive (shear-induced turbulence) processes almost compensate for each other, letting the Lagrangian term control the evolution of the angular velocity profile. In those models where turbulence cannot develop, meridional circulation dominates the transport of chemicals and AM (model M1). The dominant transport process for AM can thus differ from the process controlling the transport of chemicals. It can also vary along the evolution.

6. Signatures of mixing

6.1. Structure evolution

Through the transport of chemicals, in particular of those contributing to the nuclear energy production and the opacity, rotation may indirectly affect the evolution of stars in terms of lifetimes, luminosities, and effective temperatures. Centrifugal forces can also affect the structure, but this effect is negligible for the low rotation rates considered here.

6.1.1. Main sequence

Figure 1 presents the Hertzsprung-Russell (HR) diagram for the models listed in Table 1. Models M 0 to M3 can hardly be distinguished in the figure. Due to their low initial rotation velocity and the absence of braking to pump AM, models M1 to M3 present very weak differential rotation resulting in inefficient mixing during the MS phase ($D_{\rm tot} \approx 10^2$–10^3 cm^2 s^{-1}); their evolution, as well as their chemical structure, is thus only scarcely affected by rotation-induced mixing. Table 3 presents the main evolutionary characteristics of our models. The luminosity and effective temperature at the turn-off, as well as the time spent on the MS, are similar in slowly rotating (M1–M5) and standard (M 0) models.

Model M6 deviates from the standard and slow-rotating tracks. In this model, the strong braking applied during the first million years spent on the MS creates a strong differential rotation inside the star leading to an efficient transport of the chemicals (see Eq. (7)). In this case, as helium diffuses outwards, the opacity is globally lower and the star consequently bluer and more luminous. As a result of fuel replenishment due to efficient rotational mixing, the H-burning phase also lasts for ≈ 400 Myr longer in model M6, which is thus older at the turn-off compared to the other rotating models (Table 3).

Table 3. Main evolutionary features of the models presented in Table 1. TO index stands for *turn-off values*. $M_{\rm BCE,DUP}$ is the mass coordinate associated with the deepest extension of the convective envelope during the first dredge-up. $\Delta t_{\rm bump}$ is the time needed for the entire HBS to pass through the μ-discontinuity left by the 1st DUP.

Model	0	1	2	3	4	5	6
$t_{\rm TO}$ (Gyr)	11.11	11.20	11.21	11.21	11.21	11.21	11.61
$L_{\rm TO}$ ($L_\odot$)	3.35	3.34	3.35	3.35	3.35	3.35	3.55
$T_{\rm eff,TO}$ (K)	6534	6547	6543	6543	6543	6543	6582
$\upsilon_{\rm TO}$ (km s^{-1})	0	3.88	3.90	3.89	3.85	3.95	5.71
$M_{\rm BCE,DUP}$ ($M_\odot$)	0.306	0.303	0.304	0.306	0.304	0.307	0.306
$L_{\rm bump}$ ($L_\odot$)	107	101	109	113	103	110	114
$T_{\rm bump}$ (K)	4899	4919	4897	4887	4910	4896	4897
$\Delta t_{\rm bump}$ (Myr)	4.87	7.14	7.75	6.28	5.75	6.68	7.73

For all our rotating models, the surface velocity at the end of the MS is lower than 6 km s^{-1}, in fair agreement with the upper limits derived for globular clusters MS stars (Lucatello & Gratton 2003). During the MS evolution, the surface rotation velocity remains almost constant in models M1 to M5. They are slowed from 5 km s^{-1} on the ZAMS to ≈ 4 km s^{-1} at the turn-off mainly due to the structural readjustment that becomes important at the end of this phase. Model M6 undergoes magnetic braking on the MS so that its rotational velocity has already dropped below ≈ 6 km s^{-1} when the model reaches the middle of the main sequence (i.e. for $X_{\rm c} \simeq 0.5$). This velocity decreases further due to the efficient transport of AM in the radiative interior, and reaches 5.7 km s^{-1} at the turn-off.

6.1.2. Red giant branch

The large increase in radius accompanying the deepening of the convective envelope during the 1st DUP, combined with global conservation of AM, leads to very efficient braking of the surface layers and spin-up of the core. All our rotating models have surface velocities lower than 1 km s^{-1} at the end of the dredge-up (including model M6 for which we have $\upsilon_{\rm ZAMS} = 110$ km s^{-1}). In models M1, M2, M4, and M6, for which the total diffusion coefficient for chemicals is higher than the molecular viscosity at the base of the envelope, the 1st DUP is deeper compared to the standard case. These variations in the depth of the 1st DUP (Table 3) remain small, however, and will not significantly affect the surface abundance patterns at this phase (see Sect. 6.2, Fig. 15).

In the following we will refer to the *bump luminosity* as the *luminosity of the model when the mass coordinate of the maximum energy production inside the HBS is equal to* $M_{\rm BCE,DUP}$. Figures 11–13 present selected abundance profiles and the mean molecular weight gradient $\nabla_\mu = \partial \ln \mu / \partial r$, before and after the *bump* inside models M 0, M1, and M6, respectively. The peak amplitude $\nabla_{\mu,{\rm c}}$ in the μ-gradient profile at $M_r = M_{\rm BCE,DUP}$ (indicated by an arrow on the left panels) decreases with increasing degrees of mixing. In the non-rotating model, this peak is a signature of the deepest penetration of the convective envelope during the first dredge-up, and the corresponding $\nabla_{\mu,{\rm c}}$ value is $\simeq 10^{-11}$ (Fig. 11). In the rotating models, the peak is spread out due to the ongoing transport of the chemicals, and it varies between $\nabla_{\mu,{\rm c}} \simeq 3 \times 10^{-12}$ (Fig. 12) and $\nabla_{\mu,{\rm c}} \simeq 5 \times 10^{-13}$ (Fig. 13). The amplitude of $\nabla_{\mu,{\rm c}}$ directly reflects the strength of the diffusion coefficient in this area (see Figs. 4 and 6). According to Charbonnel et al. (1998) the regions where $\nabla_\mu \geq 1.5 \times 10^{-13}$

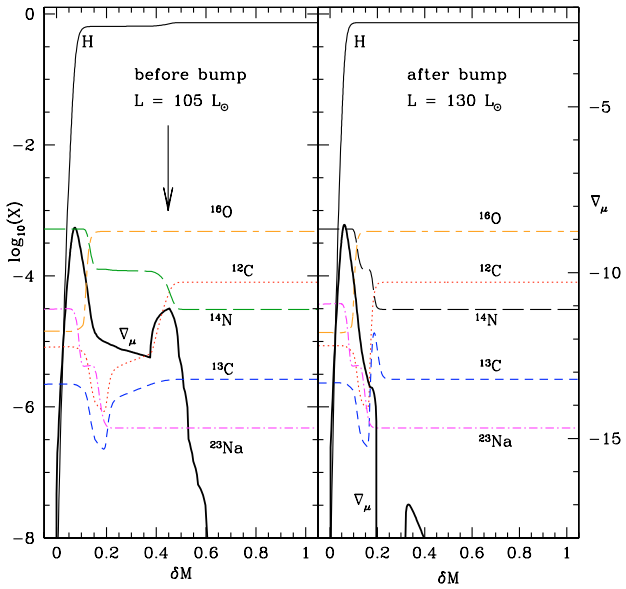

Fig. 11. Logarithm of the mass fraction profiles of H, ^{12}C, ^{13}C, ^{14}N, ^{16}O, ^{23}Na and of the mean molecular weight gradient $\nabla_\mu = \mathrm{d}\ln\mu/\mathrm{d}r$ (bold line) as a function of the reduced mass inside a 0.85 $M_\odot$, Z = 0.0005 standard stellar model M 0. The panels represent the profiles of these elements in the HBS just before (i.e. before the HBS contacts the μ-discontinuity left by the 1st DUP) and after (i.e. once the mass coordinate at the base of the HBS is larger than $M_{\mathrm{BCE,DUP}}$) the *bump*. In the left panel, the down-going arrow indicates the mass coordinate of maximum penetration of the CE during the 1st DUP.

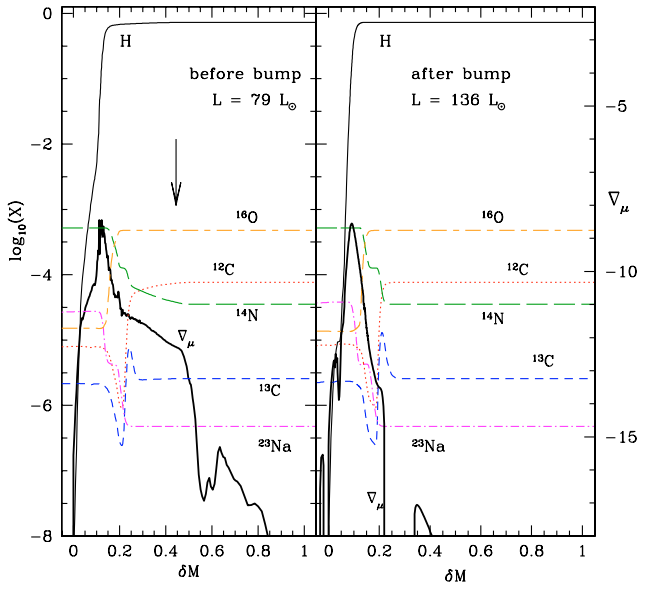

Fig. 12. Same as Fig. 11 for our rotating reference model M1.

should not be affected by the extra-mixing acting below the CE. Therefore, even the low value of $\nabla_{\mu,\mathrm{c}}$ found in model M6 can prevent mixing from acting freely below $\delta M \approx 0.5$. Let us finally emphasise, that, although the amplitude of the diffusion coefficients may be locally increased due to numerical instabilities and could artificially lower the mean molecular gradient in that region, the reproducibility and constancy of the μ-barrier spreadover indicates that this feature is not a numerical artifact.

To evaluate the "observational" impact of rotational mixing on the luminosity function's *bump*, we computed theoretical luminosity functions (hereafter LF) for each of our models (see

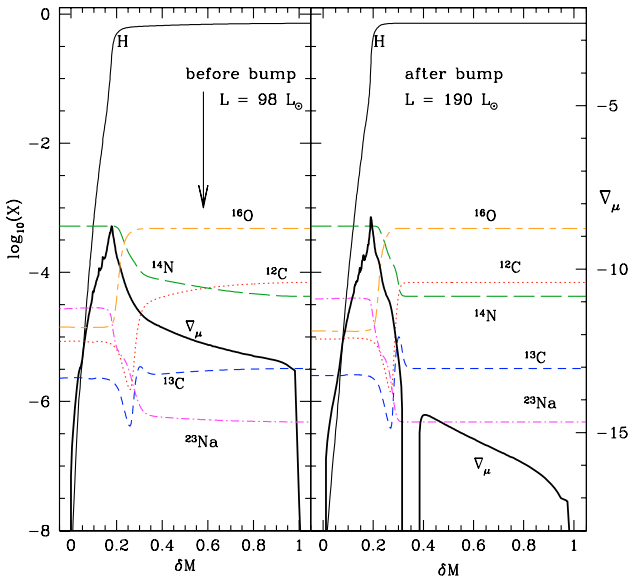

Fig. 13. Same as Fig. 11 for model M6.

Fig. 14). These theoretical LF represent the time spent in each bin of magnitude V by models on the RGB with magnitudes lower than $V = 16.6$. We chose this cut-off so as to compare the models' predictions with the observed luminosity function of the globular cluster M 13 as given by Cho et al. (2005).

To determine the V magnitude associated with a given luminosity L, we used the classical magnitude-luminosity relation

$$V = M_{\mathrm{bol},\odot} - 2.5\log(L/L_\odot) - \mathrm{BC} + (m-M)_V.$$

For M 13, we adopted a distance modulus $(m-M)_V = 14.48$, following Cho et al. (2005), and a bolometric correction BC = −0.253, according to the value given by Girardi et al. (2002) for [Fe/H] = −1.5, $T_{\mathrm{eff}} = 5000$ K and $\log g = 2$. $M_{\mathrm{bol},\odot} = 4.76$ according to Cox (2000).

Figure 14 emphasises the following points:

1. the *bump* clearly appears for all models in spite of the numerical noise present at higher magnitudes in models M2 and M6. When the μ-barrier has been efficiently eroded, the bump is less pronounced in the LF;
2. the predicted LF for models with a low degree of mixing (namely M1, our reference model, and M3, with $E_\mu = 0$) are similar to the one obtained for the standard model M 0. In the case of model M3, the diffusion coefficient in the outer HBS always remains small prior to the *bump* (i.e. $D_{\mathrm{tot}} \leq 5 \times 10^3$ cm^2 s^{-1}). This allows preservation of a strong μ-gradient that is responsible for the clear signature in the LF. A similar effect explains the LF for model M1, where transport efficiency is always low in the radiative zone.
3. In rotating models, the *bump* occurs at higher luminosity compared to the standard model M 0.

6.2. Abundances

In Sect. 6.1, we mentioned the lowering of the mean molecular weight barrier left by the 1st DUP in rotating models M1 and M6. Figure 12 shows the erosion of ^{12}C and ^{14}N profiles as a result of rotational mixing. However, this chemical diffusion does not affect the surface abundances significantly and we report only a minor increase in ^{14}N anti-correlated with a decrease in ^{12}C compared to the standard case.

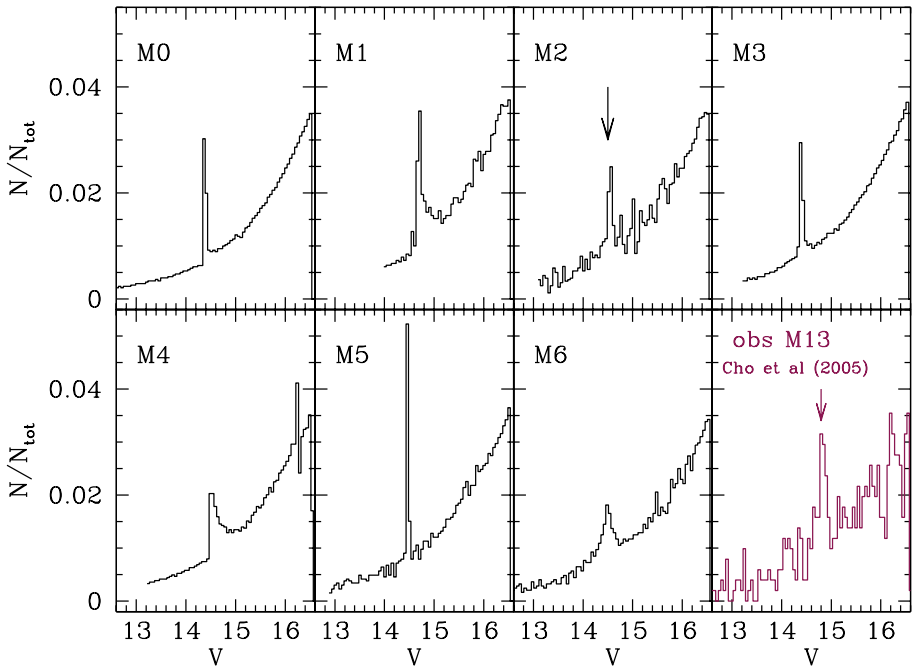

Fig. 14. Normalised theoretical luminosity function in V for the models presented in Tables 1 and 3. These histograms represent the time spent in each magnitude (luminosity) bin as a function of visual magnitude V. The ordinates are normalised to the total time spent on the portion of the RGB where $V \leq 16.6$. This limit has been chosen in order to have the same normalisation as in the observational case presented in the 8th panel (*low right*). The observed normalised luminosity function is based on Cho et al. (2005). The arrows in panels 3 and 8 indicate the position of the *bump*.

In Model M6 the higher degree of differential rotation at the base of the CE feeds the turbulent shear-induced mixing. The outer ^{14}N plateau is erased and the nitrogen mass fraction in the CE is increased relative to the standard case. ^{13}C also diffuses outwards and the peak around $\delta M = 0.3$ is flattened out. Although the mean molecular weight at the depth of deepest penetration of the CE is much lower than in the standard model, D_v (which dominates the transport) decreases rapidly from 10^9 cm^2 s^{-1} just below the CE down to $\approx 10^5$ cm^2 s^{-1} in the chemically inhomogeneous regions of the outer HBS (Fig. 8). Mixing is thus confined to a narrow region located just below the CE, where the chemical profiles are flat. According to Charbonnel (1995) and Denissenkov & VandenBerg (2003), diffusion coefficients as large as $\approx 4 \times 10^8$ cm^2 s^{-1} are needed to connect the HBS with the CE and to modify the surface abundances. However this configuration is never reached in our self-consistent models.

We reach similar conclusions for the other rotating models, since at the *bump*, the diffusion coefficients have the same magnitude, and are too small to affect the surface abundance composition. This is clearly illustrated in Fig. 15, where we present a comparison of the temporal evolution of lithium, carbon, nitrogen, and carbon isotopic ratios obtained in our models with homogeneous observational data for field stars with [Fe/H] $\in [-2; -1]$. While variations associated with the 1st DUP are satisfactory and rotating models tend to more closely agree with observations, no further variations were obtained after the *bump*. Let us note that model M6 leads to the destruction of lithium already on the MS (because of strong mixing associated with the shear in the absence of any compensating mechanism) in contradiction with the observations. This situation is similar to the one encountered in Pop I stars on the red side of the lithium dip. For a complete discussion of this problem, the reader is referred to Talon & Charbonnel (1998), as well as to Talon & Charbonnel (2005) and Charbonnel & Talon (2005), which describe how internal gravity waves could help resolve this issue in Pop II stars.

Regarding lithium on the RGB, the mixing rates associated with shear-induced turbulence do not allow the triggering of the Li-flash as proposed by Palacios et al. (2001) to consistently explain the low percentage of lithium-rich giants at the *bump* luminosity. Indeed, in this scenario, an initial mixing rate of about 10^9 cm^2 s^{-1} is needed in the region of the ^{7}Be peak region in order for it to diffuse outwards and decay into ^{7}Li in a region where this nuclide will efficiently capture protons and give rise to an energetic runaway called the "Li-flash". We never get such high mixing rates in the radiative interior of our models.

The present description of the extra-mixing process in RGB stars does not allow the models to reproduce the observed abundance anomalies in upper RGB stars, and does not validate the Li-flash scenario for Li-rich RGB.

7. Comparison with previous works

In this paper we have presented the first models of rotating low-mass stars that take into account rotational transport by meridional circulation and shear turbulence coupled self-consistently to the structural evolution from the ZAMS to the upper RGB. A detailed study of the input physics associated with the rotational transport of angular momentum and chemicals allowed us to assess the impact of various physical ingredients on the extension and magnitude of mixing along the giant branch. Let us now compare our predictions with others from the literature.

1. **Angular momentum evolution**

   With regard to the evolution of the angular velocity profile, we assumed solid body rotation on the ZAMS in all our models and then let angular momentum be transported by meridional circulation and shear-induced turbulence. At the turn-off, this leads in all cases to differential rotation in the radiative interior and to a slowly rotating convective envelope. *Beyond the turn-off, the angular velocity below the CE is determined by the assumed rotation law in the CE. Both the absolute value of* $\Omega_{\rm BCE}$ *and the degree of differential rotation (and hence mixing) in the radiative zone are maximised after completion of the 1st DUP in the case of a*

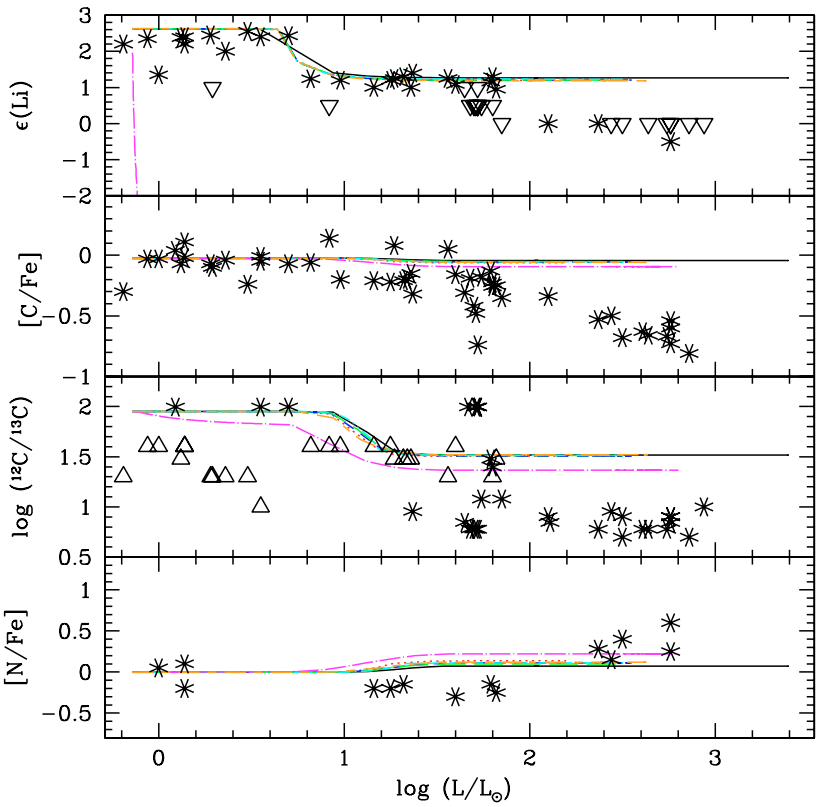

Fig. 15. Evolution of the lithium abundance ($\epsilon(^{7Li})$), the carbon isotopic ratio $^{12}C/^{13}C$, [C/Fe] and [N/Fe] as a function of the luminosity logarithm for the models presented in Table 1. Line encoding is the same as in Fig. 1. Black asterisks are actual measurements, open upward triangles are *lower* limits, and open downward triangles are *upper* limits. Observational data are from Gratton et al. (2000) for field stars in the metallicity range [Fe/H] $\in [-2; -1]$.

differentially rotating CE ($j_{CE}(r)$ = const.). This supports the conclusions anticipated by other authors. In 1979, Sweigart & Mengel conjectured that differential rotation in the convective envelope of a red giant with homogeneous specific angular momentum could be necessary to provide enough rotational mixing at the *bump*. Recently, Chanamé et al. (2005), using a "maximum mixing approach", reach the same conclusion from considerations on the global AM budget. They also indicate that, if Ω has to be described by a power law, it is not necessarily with a -2 index (e.g. uniform specific angular momentum). As we mentioned in Sect. 3.5, assuming uniform specific angular momentum is a first approximation, so we may expect better estimates of the CE rotation regime from direct numerical simulations.

In their work, Chanamé et al. (2005) nonetheless insist on the fact that in order for rotational mixing to reproduce the observed abundance anomalies of low-mass Pop II RGB stars, they need to assume unrealistically high rotation velocities at the turn-off. This is a conclusion that we also reach in our complete computations. Differential rotation in the radiative region separating the HBS from the CE increases as the CE retreats after the DUP. However, *the self-consistent evolution of the rotation profile for realistic surface velocities at all phases leads to transport coefficients that are too low by 3 orders of magnitude compared to what is expected from parametric studies (Weiss et al. 2000; Denissenkov & VandenBerg 2003) to alter the surface chemical composition beyond the* bump luminosity *and reproduce the observed patterns.*

In this work, we did not force the specific angular momentum to *have the same value at all times in the convective envelope*, as was done by Denissenkov & Vandenberg (2003). Under such an assumption, the specific angular momentum within the CE remains at the same level during the 1st DUP as at the turn-off, which results in an increase in the differential rotation and mixing below the CE. On the contrary, in the models M2 to M6 presented here, when the CE deepens during the 1st DUP, it dredges up material with lower specific angular momentum, and j_{CE} (which is the same in each mass shell within the CE) drops as can be seen from Fig. 3. As a result, the angular velocity and the differential rotation are lower at the *bump*. Beyond the completion of the 1st DUP, j_{CE} continues to evolve slightly due to angular momentum transfer with the underlying radiative zone, but does not vary significantly anymore. Assuming *no variation in space* of the specific angular momentum in the CE after the turn-off appears to be very different from assuming *no variation with time* of this same quantity. This latter assumption, when combined with strong differential rotation in the radiative interior on the MS, is an ad hoc way to produce strong differential rotation (and mixing) at the *bump*.

Although Denissenkov and collaborators (Denissenkov & Tout 2000 (DT00); Denissenkov & VandenBerg 2003 (DV03)) have also searched for a solution to the RGB abundance anomaly problem in terms of rotational mixing by meridional circulation and shear turbulence, they reach very different conclusions in terms of the evolution of the surface abundance pattern on the RGB. As a matter of fact, their transport coefficients are very similar to ours in terms of shape, but they get much higher rotation velocities and differential rotation rates than we do, resulting in higher mixing rates at all phases.

The origin of the differences is difficult to assess although several points are certainly critical. First of all the self-consistency of the treatment of rotational transport within the stellar evolution code, which allows the retro-action of AM and chemical transport on the structure at each evolutionary step, seems to be crucial. Although DT00 solved Eq. (1)

using the Maeder & Zahn (1998) formalism, this was done outside their evolution code in a post-processing way. In addition they imposed an angular velocity profile at the *bump* (up to this point, their model does not consider any transport) so as to reproduce the observed anomalies in the globular cluster M 92. As a result they obtain very high mixing rates able to change the O and Na surface abundances. As mentioned in Sect. 1, recent observations in different GCs indicate that the O-Na anti-correlation also exists in turn-off stars, with a similar spread to RGB stars. This strongly suggests that this pattern is predominantly of primordial origin, and that there is no need for the evolutionary models to reproduce it, at least when considering an average GCRGB star[5]. In our approach, the angular velocity profile at the *bump* is not assumed but stems from the evolution (due to structural readjustments and rotational transport) from the ZAMS. It is by no means a free parameter that can be tuned at the *bump*.
Another important difference concerns the assumption made by DV03 on the evolution of the angular velocity at the base of the CE (in this paper they do not consider the rotational transport of AM, and they apply the rotational transport to the chemicals only from the *bump* on). In order to get the "right" Ω profile at the *bump*, they need to impose the constancy of the specific angular momentum *from the ZAMS up to the RGB tip*. We consider that this strong assumption is unphysical.

As a consequence, the work by Denissenkov and collaborators should not be considered as proof of the efficiency of rotational transport by meridional circulation and shear-induced turbulence in modifying the surface abundance pattern of low-mass RGB stars. It does, however, show what the angular momentum distribution at the *bump* should be in a rotating star for shear-induced turbulence to produce the required amount of mixing in these objects.

2. **Description of the turbulence**

We have investigated the effects of using different prescriptions for both the horizontal and vertical turbulent diffusion coefficients during the RGB evolution. *Although some differences arise depending on the adopted descriptions of turbulence, their effects on the transport of chemical species at the* bump *and beyond are marginal*. Concerning the choice of $\nu_{\rm h}$, the MPZ04 prescription predicts a higher value which ensures the validity of the shellular rotation scheme, a condition that is not always fulfilled when using Zahn92 prescription. The MPZ04 prescription also (over-)quenches the efficiency of meridional circulation and that of the μ-currents. Regarding the choice of $\nu_{\rm v}$, contrary to the expectations of Denissenkov & Tout (2000), the TZ97 prescription for $\nu_{\rm v}$ does not lead to efficient mixing throughout the entire radiative zone, nor does it contradict the observations when implemented in a self-consistent scheme where μ-gradients are taken into account. The observations in low-mass RGB stars do not allow any discrimination between the MM96 and the TZ97 prescriptions for $\nu_{\rm v}$, and the use of the former prescription in order to prevent any mixing in the outer HBS prior to the *bump*, as advocated by Denissenkov and collaborators, is not justified. Let us also recall that the TZ97 prescription leads to a much better agreement in the case of massive stars.

3. **μ-currents and μ-gradients**

Several important results obtained from our models concern the effect of mean molecular weight gradients (μ-gradients) on the rotational transport.

In this paper and in Paper I, we have studied the effect of the μ-gradients on the main sequence. In Sect. 5.3, we have shown that, if the present low-mass RGB stars were slow rotators on the ZAMS, shear-induced turbulence could not develop in the radiative interior during the main sequence. In this case, and independent of the prescription used for the turbulent diffusion coefficients, the μ-currents have no effect since rotational mixing is negligible. For model M6, a fast rotator on the ZAMS undergoing strong braking on the main sequence, we reach the same conclusion as in Paper I when the Zahn92 prescription was used for $D_{\rm h}$: μ-currents play an important role in shaping the turn-off rotation profile. On the other hand, the use of the MPZ04 prescription for $D_{\rm h}$ reverses this conclusion, and the μ-currents are insignificant, as in the case of the slow rotators.
Beyond the turn-off, the transport erodes the μ-gradients in all our rotating models, including those with uniform angular velocity in the CE. The μ-discontinuity translates into a dip in the diffusion coefficient profiles. The less the mixing, the broader and the more persistent this feature. In models with uniform specific angular momentum in the CE, this gap is soon filled after the 1st DUP because turbulent transport is efficient enough in this region to smooth the chemical gradients. Despite the lowering of the μ-barrier, $D_{\rm tot}$ remains, however, too small to connect the outer HBS with the CE, and the surface abundance pattern is not altered prior to the *bump*. Concerning the observational consequences, spreading over of the μ-barrier lowers the luminosity function height at the *bump*, but does not erase it. *The μ-gradients are thus seemingly not entirely responsible for the lack of mixing evidence in lower RGB stars, contrary to what was conjectured by SM79 and Charbonnel (1995). A similar conclusion was reached by Chanamé et al. (2005) in their "optimised rotational mixing" approach.*

Finally, in all our rotating models, the μ-barrier associated with the HBS very efficiently prevents any mixing to connect the Na-rich layers with the outer radiative envelope. Thus, contrary to Chanamé et al. (2004a,b, 2005) and Denissenkov & VandenBerg (2003), the mixing depth does not need to be parametrised if the effects of μ-currents on the mixing are consistently taken into account.

8. Conclusion

Our self-consistent approach of rotational mixing associated with meridional circulation and shear-induced turbulence leads to two major conclusions: (1) *this formalism does not provide transport coefficients in low-mass, low-metallicity RGB stars that are large enough to explain the abundance anomalies observed both in the field and in globular clusters*; (2) *it requires differential rotation in the convective envelope*[6] *to*

[5] In the specific case of M 13, the extreme O-Na anti-correlation observed in RGB tip stars could, on the other hand, be attributed to some extreme mixing whose signature is superimposed on the primordial pattern and exacerbates it.

[6] This rotation regime is achieved in our case by imposing uniform specific angular momentum within this region.

obtain non-negligible differential rotation rates and, hence, mixing rates in the underlying radiative region.
These results point toward remaining open questions that we would like to bring to light.

The interplay between convection and rotation in extended stellar convective envelopes is still unknown, and the hypothesis of differential rotation is very attractive when the shear is the only process considered as triggering the turbulent transport of angular momentum and chemicals.

In our work, it appears that changing the angular velocity profile in the convective envelope from uniform to differential increases the degree of mixing in the underlying radiative region. This enhancement remains moderate, however, and does not lead to the large diffusion coefficients expected from parametric studies. As the shear-induced turbulence appears not to be efficient *on its own* in reproducing the observed abundance anomalies in low-mass giants independently of the rotation law in the convective envelope, we are not able at present to make any statement concerning this aspect. We nonetheless would be very interested in the use of 3D hydrodynamical direct simulations to assess the rotation regime within the extended convective envelopes of cool giants.

In their recent work, Chanamé et al. (2005) propose that the rotation regime of the convective envelopes may change during the evolution, going from solid-body during the MS to differential rotation on the RGB. Such a scheme would reconcile rotation velocities of MS and horizontal branch stars, together with abundance patterns from the MS to the RGB tip. Here again, if another physical process, such as internal gravity waves, is also able to transport angular momentum in giants and if its efficiency at all evolutionary phases depends on the initial mass, the modification of the rotation regime in the convective envelope during the giant phase would no longer be necessary.

The second point concerns the transport mechanisms associated with differential rotation. By now, only the secular shear instability has been investigated. This is mainly related to historical reasons, since Zahn's formalism was at first derived for MS stars, where this hydrodynamical instability is dominant. The structure of a giant star is, however, very far from resembling that of the Sun. We might then expect that specific features, such as nuclear burning shells, contracting radiative interior, and expanding (extended) convective envelope, favour the triggering of other hydrodynamical instabilities or physical transport mechanisms. Spruit & Knobloch (1984) advocate the possibility of the baroclinic instability being efficient in giant stars, but at present, we lack a description in the non-linear regime (e.g. in a regime associated with turbulence). This instability also depends on the degree of differential rotation but is not as sensitive to μ-gradients as the secular shear, and could thus complement the effect of secular shear in increasing the degree of mixing in regions with large μ-gradients. Other instabilities, such as the Goldreich-Schubert-Fricke (GSF) and the Solberg-Høiland, instabilities could also become non-negligible during the RGB phase.

Last but not least, and in connection with the presence of the so-called "super Li-rich giants" at the RGB *bump* (Charbonnel & Balachandran 2000, and references therein), Palacios et al. (2001) propose that the structural and nuclear response of the star to the rotation-induced mixing could cause an increase in $D_{\rm tot}$ as required to explain the abundance anomalies. This scenario involves a large release of energy due to ^{7}Li burning in the external wing of the HBS (the so-called "Li flash"). This opens up a new field of investigation concerning the reaction of meridional circulation and of the various instability to a major and local release of nuclear energy.

Our results clearly show the lack of success of secular shear *alone* to trigger a large enough amount of extra-mixing, but does not rule out rotation-induced mixing being responsible for abundance anomalies in low-mass giants. As a matter of fact, rotation remains at present the best candidate for the triggering of the extra-mixing process in these objects. Our study points toward the need for more physics, implying a revision of the coupling between rotation and convection, and toward the treatment of any other physical processes likely to contribute to transport angular momentum, including the hydrodynamical instabilities neglected before.

Acknowledgements. The comments of the referee allowed improvement of the initial version of this paper. L.S. is an FNRS research associate. A.P. acknowledges financial support from the ESA PRODEX contract 96009. C.C. is supported by the Swiss National Science Foundation. We thank the French Programme de Physique Stellaire (PNPS) and Programme National Galaxies (PNG) for travel support.
We dedicate this work to the memory of our friend Dr. Manuel Forestini.

Appendix A: Detailed expressions for the components E_Ω and E_μ in Eq. (2)

Maeder & Zahn (1998) derived a generalised expression of the meridional circulation velocity U_r, taking into account the effects of μ-gradients and non-stationarity and of a general equation of state, which was revised and corrected in Denissenkov & Tout (2000).

Here, we reproduce the detailed expressions of the E_Ω and E_μ terms appearing in Eq. (2). Equations (A.1) and (A.2) correspond to corrected versions of Eqs. (4.30) and (4.42) found in Maeder & Zahn (1998).

$$\begin{aligned} E_\Omega \;=\; & 2\left[1-\frac{\overline{\Omega^2}}{2\pi G\overline{\rho}}-\frac{(\overline{\varepsilon}+\overline{\varepsilon}^{\rm grav})}{\varepsilon_{\rm m}}\right]\frac{\tilde{g}}{\overline{g}} \\ & -\frac{\rho_{\rm m}}{\overline{\rho}}\left\{\frac{r}{3}\frac{\rm d}{{\rm d}r}\left[H_{\rm T}\frac{\rm d}{{\rm d}r}\left(\frac{\Theta}{\delta}\right)-\chi_{\rm T}\frac{\Theta}{\delta}+\left(1-\frac{1}{\delta}\right)\Theta\right]\right. \\ & \left.-\frac{2H_{\rm T}}{r}\left(1+\frac{D_{\rm h}}{K}\right)\frac{\Theta}{\delta}+\frac{2}{3}\Theta\right\}-\frac{(\overline{\varepsilon}+\overline{\varepsilon}^{\rm grav})}{\varepsilon_{\rm m}}\left[H_{\rm T}\frac{\rm d}{{\rm d}r}\left(\frac{\Theta}{\delta}\right)\right. \\ & \left.+\left(f_\varepsilon\varepsilon_{\rm T}-\chi_{\rm T}\right)\frac{\Theta}{\delta}+\left(2-f_\varepsilon-\frac{1}{\delta}\right)\Theta-\frac{\overline{\Omega^2}}{2\pi G\overline{\rho}}\Theta\right] \\ & -\frac{\overline{\Omega^2}}{2\pi G\overline{\rho}}\Theta+\frac{M_*}{L}\frac{C_{\rm p}T}{\delta}\frac{\partial\Theta}{\partial t} \end{aligned} \tag{A.1}$$

and

$$\begin{aligned} E_\mu \;=\; & \frac{\rho_{\rm m}}{\overline{\rho}}\left\{\frac{r}{3}\frac{\rm d}{{\rm d}r}\left[H_{\rm T}\frac{\rm d}{{\rm d}r}\left(\frac{\varphi}{\delta}\Lambda\right)-\left(\chi_\mu+\frac{\varphi}{\delta}\chi_{\rm T}+\frac{\varphi}{\delta}\right)\Lambda\right]\right. \\ & \left.-\frac{2H_{\rm T}}{r}\frac{\varphi}{\delta}\Lambda\right\}+\frac{(\overline{\varepsilon}+\overline{\varepsilon}^{\rm grav})}{\varepsilon_{\rm m}}\left[H_{\rm T}\frac{\rm d}{{\rm d}r}\left(\frac{\varphi}{\delta}\Lambda\right)+f_\varepsilon\left(\frac{\varphi}{\delta}\varepsilon_{\rm T}+\varepsilon_\mu\right)\right. \\ & \left.-\chi_\mu-\frac{\varphi}{\delta}(\chi_{\rm T}+1)\Lambda\right]. \end{aligned} \tag{A.2}$$

In these expressions we have used the following notations:

$$H_{\rm T}=\frac{-{\rm d}r}{{\rm d}\ln T}$$

is the temperature scale height;

$$K=\frac{\chi}{\rho C_{\rm p}}=\frac{4acT^3}{3\rho^2\kappa C_{\rm p}}$$

is the thermal diffusivity; and χ is the thermal conductivity. Also $\overline{\varepsilon}$ and $\overline{\varepsilon}^{\rm grav}$ are the means over an isobar of the nuclear and gravitational energy, respectively, and

$$f_\varepsilon \equiv \overline{\varepsilon}/(\overline{\varepsilon} + \overline{\varepsilon}^{\rm grav})$$

represents the nuclear fraction of energy. $\varepsilon_{\rm m} = L(r)/M(r)$ and $\rho_{\rm m} = M(r)/(4\pi r^3/3)$ are the mean total energy and the mean density inside a sphere of radius r.

$$\chi_\mu = \left(\frac{\partial \ln \chi}{\partial \ln \mu}\right)_{P,T}, \qquad \chi_{\rm T} = \left(\frac{\partial \ln \chi}{\partial \ln T}\right)_{P,\mu}$$

are logarithmic derivatives of the thermal conductivity χ, and

$$\varepsilon_\mu = \left(\frac{\partial \ln \varepsilon}{\partial \ln \mu}\right)_{P,T}, \qquad \varepsilon_{\rm T} = \left(\frac{\partial \ln \varepsilon}{\partial \ln T}\right)_{P,\mu}$$

are the logarithmic derivatives of the nuclear energy.

$$\varphi = \left(\frac{\partial \ln \rho}{\partial \ln \mu}\right)_{P,T}, \qquad \delta = -\left(\frac{\partial \ln \rho}{\partial \ln T}\right)_{P,\mu}$$

are derived from the equation of state using the notation by Kippenhahn & Weigert (1994).

The term $\frac{\overline{\Omega^2}}{2\pi G\overline{\rho}}\Theta$ in Eq. (A.1) is neglected because it is of order 2 in Ω^2, contrary to the other terms that are of order 1.

References

Alexander, D. R., & Ferguson, J. W. 1994, ApJ, 437, 879
Angulo, C., Arnould, M., Rayet, M., et al. 1999, Nucl. Phys. A656, 3
Balachandran, S., & Carr, J. 2003, in CNO in the Universe, ed. C. Charbonnel, D. Schaerer, & G. Meynet, ASP Conf. Ser., 304, 101
Ballot, J., Brun, A. S., & Turck-Chièze, S. 2004, SF2A-2004 meeting held in Paris, France, June 14–18, 2004, ed. F. Combes, D. Barret, T. Contini, F. Meynadier, & L. Pagani (EDP Sciences), Conf. Ser., 266
Bao, Z. Y., Beer, H., Käppeler, F., et al. 2000, At. Data Nucl. Data Tables, 76, 70
Bellman, S., Briley, M., Smith, G., & Claver, C. 2001, PASP, 113, 326
Boothroyd, A. I., & Sackmann, I. J. 1999, ApJ, 510, 232
Briley, M., & Cohen, J. 2001, AJ, 122, 242
Browning, M. K., Brun, A. S., & Toomre, J. 2004, ApJ, 601, 512
Carretta, E., Gratton, R. G., & Sneden, C. 2000, A&A, 356, 238
Caughlan, G. R., & Fowler, W. A. 1988, Atomic Data Nucl. Data Tables, 40, 283
Chaboyer, B., & Zahn, J.-P. 1992, A&A, 253, 173
Chanamé, J., Pinsonneault, M., & Terndrup, D. 2004a, IAU Symp., 215, ed. A. Maeder, & P. Eenens
Chanamé, J., Pinsonneault, M., & Terndrup, D. 2004b, to appear in Chemical Abundances and Mixing in Stars in the Milky Way and its Satellites, ed. L. Pasquini, & S. Randich, ESO Astrophysical Symposia (Springer)
Chanamé, J., Pinsonneault, M., & Terndrup, D. 2005, ApJ, 631, 540
Charbonnel, C. 1994, A&A, 282, 811
Charbonnel, C. 1995, ApJ, 453, L41
Charbonnel, C. 2005, Proc. IAU Symp., 228, in press
Charbonnel, C., & do Nascimento, J. D. 1998, A&A, 336, 915
Charbonnel, C., & Balachandran, S. 2000, A&A, 359, 563
Charbonnel, C., & Talon, S. 2005, Science, 309, 2189
Charbonnel, C., Brown, J. A., & Wallerstein, G. 1998, A&A, 332, 204
Charbonnel, C., Deliyannis, C. P., & Pinsonneault, M. 2000, The Light Elements and Their Evolution, IAU Symp., 198, 87
Cox, A. N. 2000, Allen's astrophysical quantities, 4th edn., ed. A. N. Cox (New York: AIP Press; Springer)
Da Costa, G. C., Cannon, R., Croke, B., & Norris, J. 2004, Mem. S. A. It., 75, 370
Cho, D.-H., Lee, S.-G., Jeon, Y.-B., & Sim, K. J. 2005, AJ, 129, 1922
Decressin, T., & Charbonnel, C. 2005, IAU Symp., 228, 395
Denissenkov, P. A., & Tout, C. A. 2000, MNRAS, 316, 395
Denissenkov, P. A., & VandenBerg, D. A. 2003, ApJ, 593, 509
Denissenkov, P. A., & Herwig, F. 2003, ApJ, 590, L99
Denissenkov, P. A., & Herwig, F. 2004, ApJ, 612, 1081
Endal, A. S., & Sofia, S. 1976, ApJ, 210, 184
Endal, A. S., & Sofia, S. 1978, ApJ, 220, 279
Geisler, D., Smith, V. V., Wallerstein, G., Gonzalez, G., & Charbonnel, C. 2005, AJ, 129, 1428
Gilroy, K. K. 1989, ApJ, 347, 835
Gilroy, K. K., & Brown, J. 1991, ApJ, 371, 578
Girardi, L., Bertelli, G., Bressan, A., et al. 2002, A&A, 391, 195
Gratton, R. G., Sneden, C., Carretta, E., & Bragaglia, A. 2000, A&A, 354, 169
Gratton, R. G., Bonifacio, P., Bragaglia, A., et al. 2001, A&A 369, 87
Grevesse, N., Noels, A., & Sauval, A. J. 1996, ASPC, 99, 117
Grundahl, F., Briley, M., Nissen, P. E., & Feltzing, S. 2002, A&A, 385, L14
Heger, A., Langer, N., & Woosley, S. E. 2000, ApJ, 528, 368
Horiguchi, T., Tachibana, T., & Katakura, J. 1996, Chart of the Nuclides (Japanese Nuclear Data Committee and Japan Atomic Energy Research Institute Nuclear Data Center)
Hubbard, W. B., & Lampe, M. 1969, ApJS, 18, 297
Iben, I. Jr. 1965, ApJ, 142, 1447
Iben, I. Jr. 1975, ApJ, 196, 525
Iglesias, C. A., & Rogers, F. J. 1996, ApJ, 464, 943
Itoh, N., Mitake, S., Iyetomi, H., & Ichimaru, S. 1983, ApJ, 273, 774
Ivans, I. I., Sneden, C., Kraft, R. P., et al. 1999, AJ, 118, 1273
Johnson, C. I., Kraft, R. P., Pilachowski, C. A., et al. 2005, PASP, 117, 1308
Kawaler, S. D. 1988, ApJ, 333, 236
Kippenhahn, R., & Weigert, A. 1994, Stellar Structure and Evolution (Berlin: Springer)
Kosovichev, A. G., et al. 1997, Sounding Solar and Stellar Interiors, IAU Symp., 181, 203
Kraft, R. P., Sneden, C., Langer, G. E., & Shetrone, M. D. 1993, AJ, 106, 1490
Lucatello, S., & Gratton, R. G. 2003, A&A, 406, 691
Maeder, A. 1997, A&A, 321, 134
Maeder, A. 2003, A&A, 399, 263
Maeder, A., & Meynet, G. 1996, A&A, 313, 140 (MM96)
Maeder, A., & Meynet, G. 2000, ARA&A, 38, 143
Maeder, A., & Zahn, J.-P. 1998, A&A, 334, 1000
Mathis, S., Palacios, A., & Zahn, J.-P. 2004, A&A, 425, 243
Mestel, L. 1953, MNRAS, 113, 716
Mestel, L. 1957, ApJ, 126, 550
Meynet, G., & Maeder, A. 1997, A&A, 321, 465
Meynet, G., & Maeder, A. 2000, A&A, 361, 101
Mitake, S., Ichimaru, S., & Itoh, N. 1984, ApJ, 277, 375
Palacios, A., Charbonnel, C., & Forestini, M. 2001, A&A, 375, L9
Palacios, A., Talon, S., Charbonnel, C., & Forestini, M. 2003, A&A, 399, 603 (Paper I)
Paltrinieri, B., Ferraro, F. R., Carretta, E., & Fusi Pecci, F. 1998, MNRAS, 293, 434
Paquette, C., Pelletier, C., Fontaine, G., & Michaud, G. 1986, ApJS, 61, 177
Pilachowski, C. A., Sneden, C., & Booth, J. 1993, ApJ, 407, 699
Ramirez, S. V., & Cohen, J. G. 2002, AJ, 123, 3277
Reed, C. 1998, JRASC, 92, 36
Reid, I. 1998, AJ, 115, 204
Reimers, D. 1975, Mem. Soc. Roy. Sci. Liège, 6th Ser., 8, 369
Richard, D., & Zahn, J.-P. 1999, A&A, 347, 734
Salaris, M., Riello, M., Cassisi, S., & Piotto, G. 2004, A&A, 420, 911
Shetrone, M. D. 2003a, in CNO in the Universe, ed. C. Charbonnel, D. Schaerer, & G. Meynet, ASP Conf. Ser., 304, 137
Shetrone, M. D. 2003b, ApJ, 585, L45
Siess, L., Dufour, E., & Forestini, M. 2000, A&A, 358, 593
Sills, A., & Pinsonneault, M. 2000, ApJ, 540, 489
Smith, G. H., & Martell, S. L. 2003, PASP, 115, 1211
Smith, V. V., Hinkle, K. H., Cunha, K., et al. 2002, AJ, 124, 324
Sneden, C. 2005, Proc. IAU Symp., 228, in press
Sneden, C., Kraft, R. P., Guhathakurta, P., Peterson, R. P., & Fulbright, J. P. 2004, AJ, 127, 2162
Sweigart, A. V., & Mengel, J. G. 1979, ApJ, 229, 624 (SM79)
Sweigart, A. V., Greggio, L., & Renzini, A. 1989, ApJS, 69, 911
Talon, S., & Zahn, J.-P. 1997, A&A, 317, 749
Talon, S., & Charbonnel, C. 1998, A&A, 335, 959
Talon, S., & Charbonnel, C. 2004, A&A, 418, 1051
Talon, S., & Charbonnel, C. 2005, A&A, 440, 981
Talon, S., Zahn, J. P., Maeder, A., & Meynet, G. 1997, A&A, 322, 209 (TZ97)
Tayler, R. J. 1973, MNRAS, 165, 39
Thévenin, F., Charbonnel, C., de Freitas Pacheco, J. A., et al. 2001, A&A, 373, 905
Wallerstein, G., & Sneden, C. 1982, ApJ, 229, 624
Weiss, A., Denissenkov, P. A., & Charbonnel, C. 2000, A&A, 356, 181
Yong, D., Grundahl, F., Lambert, D. L., Nissen, P. E., & Shetrone, M. D. 2003, A&A, 402, 985
Zahn, J.-P. 1974, Stellar instability and evolution, IAU Symp., 57, 185
Zahn, J.-P. 1992, A&A, 265, 115
Zoccali, M., Cassisi, S., Piotto, G., Bono, G., & Salaris, M. 1999, ApJ, 518, L49